PASSIVE ADAPTIVE DAMPING FOR HIGH STIFFNESS-LOW MASS MATERIALS INCORPORATING NEGATIVE STIFFNESS ELEMENTS

A Dissertation

by

GENE CHA

Submitted to the Office of Graduate and Professional Studies of
Texas A&M University
in partial fulfillment of the requirements for the degree of

DOCTOR OF PHILOSOPHY

Chair of Committee,	Terry S. Creasy
Committee Members,	William C. Schneider
	Wayne N.P. Hung
	Yong-Joe Kim
Head of Department,	Andreas Polycarpou

December 2013

Major Subject: Mechanical Engineering

ABSTRACT

High stiffness / low mass materials or structures reduce structure weight in transportation, but show little inherent damping. A new composite material that exhibits high stiffness and high damping might reduce issues with vibration in mechanical systems and structures. The material comprises three constituents: negative springs, positive springs, and damping elements. These components help achieve high stiffness with passive adaptive response over a frequency range. When applying sinusoidal loads on the material, the positive/negative spring interface oscillates, but body is relatively steady. This material needs a damping element to dissipate the vibrational energy at the interface. This research proposes new damping elements with novel properties starting with the fluid pumping element from the Synthetic Multifunctional Materials program. The low-hydraulic-radius hourglass (LHG) machine modified from Hawkins' original design provides high stiffness with a high damping ability. The LHG machine pumps a fluid and dissipates energy by viscous dissipation and mass transfer. This pumping creates a hysteresis effect that indicates the energy dissipation. Stacking LHG layers using Newtonian fluids in the LHG channel or a single layer using non-Newtonian fluids can produce passive adaptive damping through a frequency range. Shear thinning fluids placed in the LHG machine's channel provide adaptive performance by changing their dynamic viscosity. Experiments show passive adaptive damping up to tan δ one with a shear thinning fluid from 0.1 to 10 Hz. Computational fluid-solid interaction studies suggest a theoretical shear thinning fluid that produces high passive adaptive damping.

DEDICATION

To my parents, Dr. Cheolho Cha, and Dr. Sija Chon, my brother, Joseph H. Cha, and my academic advisor, Dr. Terry S. Creasy.

ACKNOWLEDGEMENTS

This material is based upon work supported by Defense Advanced Research Projects Agency (DARPA) and the U.S. Army Engineer Research and Development Center under grant number W911NF-11-1-0004. I thank them for providing the financial support for performing my research.

I thank my committee chair, Dr. Terry Creasy, and my committee members, Dr. William Schneider, Dr. Yong-Joe Kim, and Dr. Wayne Hung for their education and support throughout my researches. I also want to extend my gratitude to Dr. Jyhwen Wang for his guidance in my Ph.D. defense.

Thanks also go to my lab mates, Sangjin Lee, Jaehyeuk Jeon, Roston Elwell, and Tony Yang, and the department faculty and staff for making my time at Texas A&M University a valuable experience.

Finally, thanks to my parents and brother for their encouragement and love.

TABLE OF CONTENTS

Page

LIST OF FIGURES

Page

LIST OF TABLES

Page

1 INTRODUCTION

1.1 Motivation

As we approach a scarce energy era we must make stationary and moving structures as efficient as possible. Great benefits come from using advanced high-stiffness/low-mass materials to reduce structure weight—especially in transportation. However, these materials and structures produce a new problem: they have little inherent damping. If an advanced structure could maintain its high stiffness at low mass while having high damping, we could produce structures that reduce energy use while minimizing fatigue for the structure and its contents that could be passengers or equipment.

Modern mechanical systems have an inevitable vibration issue. The vibrations cause fatigue and damage that reduces safe lifetimes. For example, vibrations affect airplanes' aluminum structures and require regular inspection to reveal fatigue cracks. Automobiles vibrate from road, wind, and powertrain effects. Dissipating the vibrational energy comforts the occupants. Polymer based foam can be deposited inside automotive closure panels to reduce and damp vibration [1]. Figure 1 shows a noise reduction shield. At launch a space vehicle produces tremendous vibrational and acoustic energy [2]. The adapter shown in Figure 2 that protects high cost space payloads needs high damping performance; however, most are light and stiff sandwich panel structures. In this research, I propose a novel damping element that works with negative/positive spring

materials systems. These systems promise high damping in across a frequency range and exhibit high stiffness at low mass.

Figure 1. A noise and vibration reduction polymer form is installed inside an automotive door panel [3].

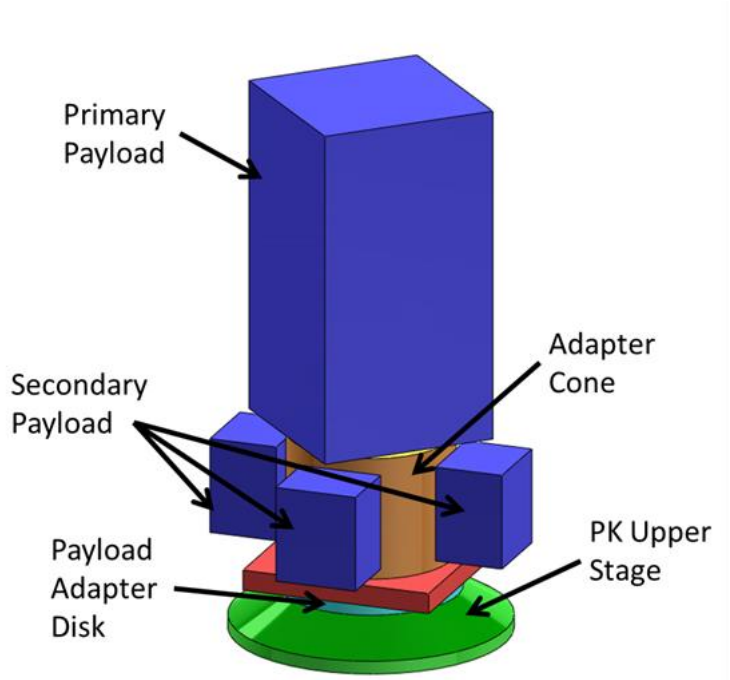

Figure 2. A simple schematic shows a space payload adapter that protects the expensive space payload such as artificial satellites from the vibrational energy (redrawn from [2]).

1.2 Overview

A new composite material that must exhibit high stiffness, low mass, and high damping is composed of three constituents: negative-stiffness materials (negative springs), positive stiffness materials (positive springs), and damping elements. This material is a passive damping composite that exhibits adaptive response over a given frequency range. The material's global mechanical behavior must integrate the individual component's behaviors. A negative-stiffness material is the primary component to this concept. The negative spring deflects more with increasing loads compared with a normal positive spring that deflects less with increasing loads. Consider a Clover spring shown in Figure 3 that responses to an applied compressive load. At first, the spring shows positive stiffness, that is, the load deflection curve slope is positive. At a critical point, the slope becomes zero and then further deflection produces a negative slope that Lakes defines as negative stiffness [4]. Finally, if the clover dome is compressed too far it snaps through. Other negative stiffness materials are a Belleville washer, and a metal bottle caps for soft drinks, e.g. Snapple.

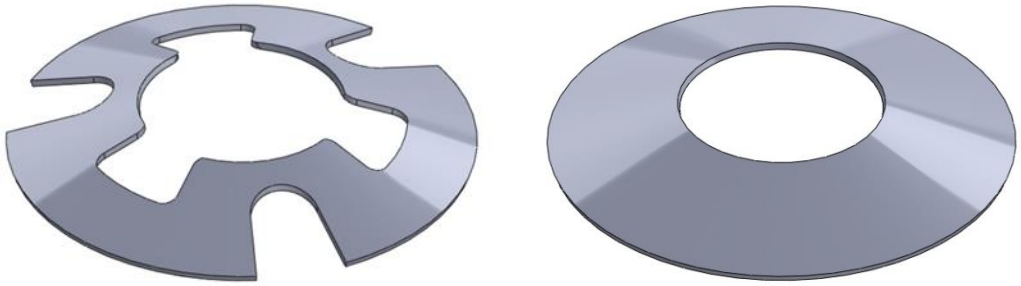

Figure 3. A Clover dome spring washer, left, and a Belleville spring washer, right, show the negative stiffness behavior.

Figure 4 shows the novel adaptive composite material concept schematically [5]. Positive spring pushes back against a compressive force, but negative spring shortens with the compressive force. Compressing upper body makes outer reaction force in positive spring and inner reaction force in negative spring. In that case the interface displaces downward in compressive force direction. Tensile input works oppositely. When applying sinusoidal input in upper body the interface oscillates, but upper body is relatively steady. To limit the +/- spring interface motion and to dissipate the vibrational energy, this material needs a damping element. The damping element can be placed at the interface between positive and negative springs where Figure 4 shows the deflections are large.

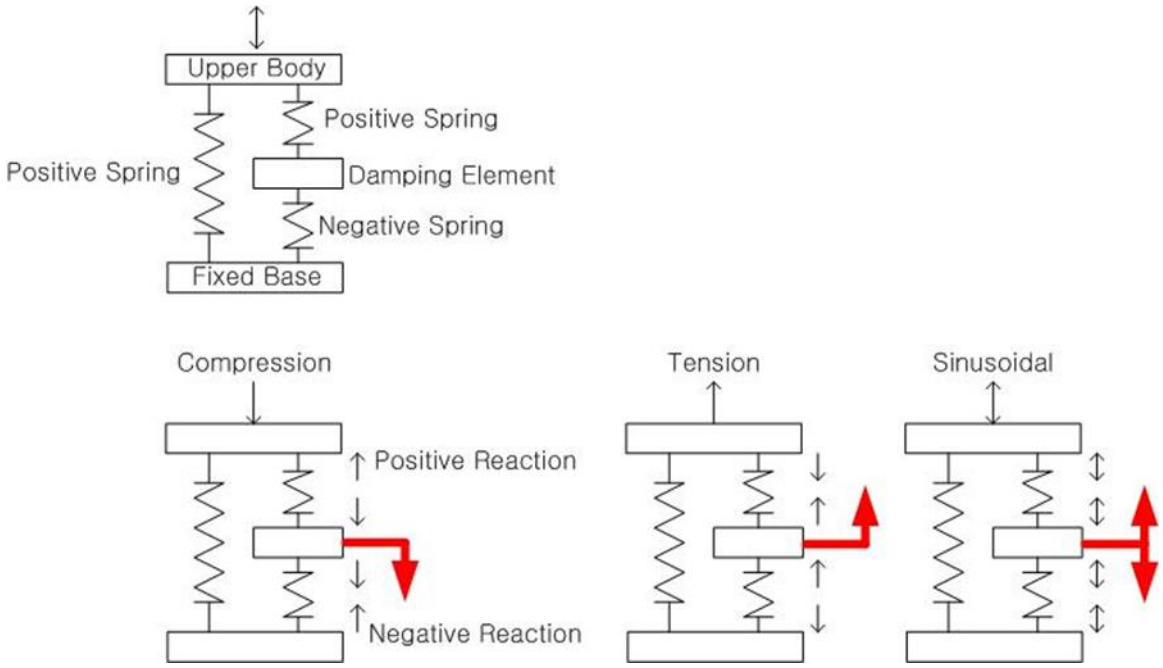

Figure 4. The adaptive composite material has damping element and positive and negative springs. The damping element in the interface between positive and negative springs compensates the sinusoidal input from the upper body. [5]

Our research target is developing new damping materials with novel properties starting with the outcome from the Synthetic Multifunctional Materials program under the Machine-Augmented Composites (MACs). The hourglass (HG) machines proposed by Hawkins are pre-buckled structures that flex as sandwich panel skins move under structural vibration [6]. Their primary purpose is to provide high stiffness with a high damping ability. The HG machines pump a fluid that dissipates energy by viscous dissipation and mass transfer. This pumping creates a hysteresis effect and hysteresis loop area indicates the energy dissipated [7]. Newtonian, and shear thinning fluids are infiltrated in the HG machine's channel. Preliminary Materials Logic program data show that the previous generation hourglass machine's damping at low frequencies outperformed typical polyurethane rubber by 37.5% [8]. Under the philosophy "make it

big, make it work, and then make it small." the adaptive composite material will be developed from the macro-scale—centimeter scale—first and reduced to millimeter scale.

1.3 Research Objective

This dissertation's objective is to develop a new Machine-Augmented Composite that adapts to varying frequencies and exhibits high stiffness and high damping simultaneously. Experiments were started under the DARPA Material Logic program. This study proposes a new hourglass machine--the Low hydraulic radius HourGlass (LHG) —as a MAC that improves the damping by pumping fluids during applied cyclic loads. This concept could be adapted to many dynamic environments and be readily incorporated into many structures. The work will follow this plan:

- Confirm the previous hourglass machine's test conditions and damping data.
- Design a new hourglass machines starting with the Low hydraulic radius Hourglass (LHG).
- Conduct cyclic tests and determine damping performance through the target frequency regime.
- Explore damping fluids that provide adaptive behavior
- Suggest the LHG's pumping conditions by fluid-solid interaction studies.
- Review and validate achieved satisfactory damping capability.
- Use experiments to model behavior beyond the 0.1 to10 Hz range.

- Suggest possible way to improve for future research.

2 BACKGROUND

2.1 Viscoelastic Damping Fundamentals

A linear viscoelastic material's damping ability can be determined either by measuring the phase angle between stress and strain sinusoids or by calculating the hysteresis loop area in the stress and strain diagram [9-11]. The tan δ is proportional to the energy loss per cycle within linear viscoelasticity [12]. Figure 5 exhibits (a) purely linear elasticity, (b) linear viscoelasticity, and (c) nonlinear viscoelasticity cases. Case (a) does not show time phase lag (left) between stress input and strain output and loop (right) is purely linear with no damping, that is, there is no hysteresis. Case (b) presents a time phase lag (Δt) that designates damping level by the ellipsoidal stress-strain diagram. The nonlinear viscoelasticity shown in case (c) has no fixed phase angle shift, but the hysteresis loop area does represent the damping quantity. The following equations present the derivation for linear viscoelastic response when the phase shift is constant. When sinusoidal strain

$$\varepsilon = \varepsilon_0 \sin(\omega t) \quad \textbf{(1)}$$

is applied on a viscoelastic system the resulting stress will be

$$\sigma = \sigma_0 \sin(\omega t + \delta) \quad \textbf{(2)}$$

Where δ is the phase angle that is 360 times frequency times Δt, ε_0 and σ_0 are constant strain and stress, ω is the circular frequency in radians per second and t is the time in seconds. Using the trigonometric identity on both equations above

$$\sin(a \pm b) = \sin(a)\cos(b) \pm \cos(a)\sin(b) \quad \textbf{(3)}$$

$$\sigma = (\sigma_0 \cos\delta)\sin\omega t + (\sigma_0 \sin\delta)\cos\omega t \quad \textbf{(4)}$$

$$\frac{\sigma}{\varepsilon_0} = (E' \sin\omega t + E'' \cos\omega t) \quad \textbf{(5)}$$

where $E' = \frac{\sigma_0}{\varepsilon_0}\cos\delta$ is the materials storage modulus and stiffness and $E'' = \frac{\sigma_0}{\varepsilon_0}\sin\delta$ is the material's loss modulus or energy dissipation ability. When E' and E'' are divided the result is

$$\tan\delta = \frac{E''}{E'} \quad \textbf{(6)}$$

Creasy developed Equation (7) that presents a relation between effective delta, δ_{eff}, and the hysteresis loop area, A_d. In the nonlinear viscoelastic case we cannot specify the tan δ as one number, but we can measure the hysteresis loop area and convert it into an δ_{eff} [7].

$$A_d = 0.1381\delta_{app}^3 + 0.0647\delta_{app}^2 + 0.7398\delta_{app} \quad \textbf{(7)}$$

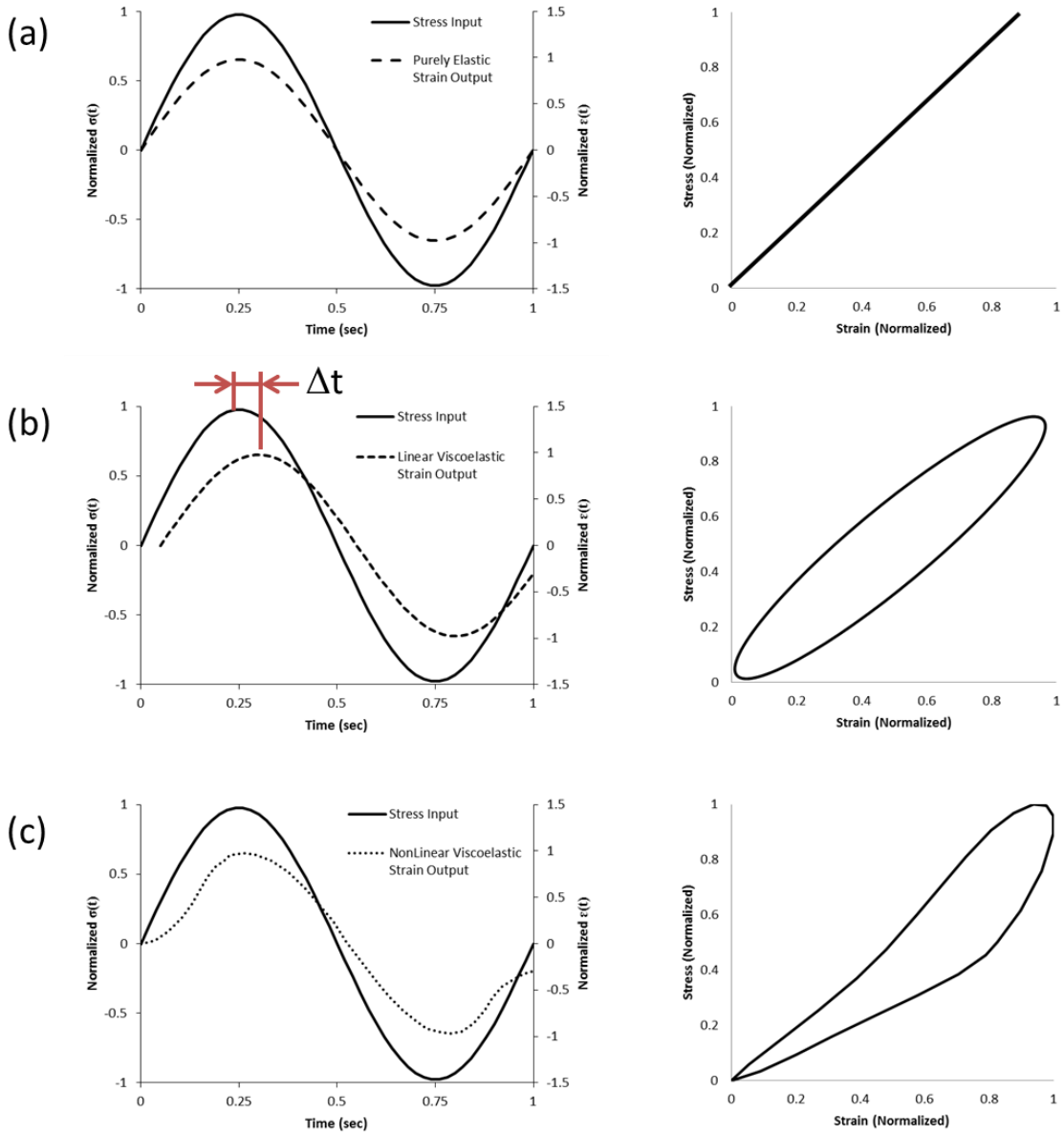

Figure 5. Plots on the left column show normalized stress and strain changes on the y axis with time on the x axis. Right column plots are hysteresis loops composed of normalized strain and stress. Sinusoidal stress and strain for a linear viscoelastic material shows the phase lag (b) unlike purely elastic material case (a). In the nonlinear viscoelasticity case (c), hysteresis loop size represents the damping level.

2.2 Passive, Active, and Adaptive Damping Defined

To achieve damping, a material or structure gets a stimulus input and provides response. Figure 6 shows various ways to obtain damping. Passive damping does not require sensors, but may react slowly and may not meet high sensitivity case. With going down the list, the system has more subtle and higher complexity.

Passive : Structure

Active : Structure + Sensor + Actuator

Smart : Structure + Sensor + Actuator + Processor

Figure 6. Smart structure architecture.

Adaptive damping commonly requires active systems, i.e. sensing with actuation. Representative example is upscale automobile shock absorbers that sense shock input from road conditions and change their setting to obtain best damping ability. The sensors are extra apparatuses that cost maintenance and gain weight additionally. Passive system that has no sensors is more reliable and less cost caused by low complexity. Kim and Singh studied a passive and adaptive hydraulic engine mount system that exhibits broad bandwidth performance up to 250 Hz [13]. Khorrami developed an adaptive passive isolator for launch vehicle payloads working in frequencies from 5 to 100Hz. His novel three degrees-of-freedom vibration isolator only allows rocking motion and compensates for varying loads caused by changes in the launch vehicle acceleration [14].

2.2.1 Damping in Conventional Materials

Conventional homogeneous isotropic materials can be energy dissipation substances. Table 1 presents various materials' damping performances. The metals exhibit low tan δ, that is, poor damping, but polymers show higher damping. General elastomers and other amorphous thermoplastic polymers with a glass transition temperature below room temperature have showed the highest damping materials. The loss modulus terms are at maximum near the glass transition [15]. Unlike crystalline matter, cross linked molecule's mobility creates relaxation mechanisms in the transition. Polymer blends' interface between components also provides a damping mechanism. High damping polymers reduce car door closing noise, engine vibration, building and bridge fatigue [16].

Table 1. Damping property in metal and polymer materials (redrawn from [17, 18]).

	Material	Frequency (Hz)	Tan δ	Testing Temperature (℃)	Testing Method
Metal	Aluminum	0.1 ~ 10	10×10^{-5}	N/A	N/A
	Al 2024-T4	100	7×10^{-4}	N/A	Bending
	Al 6063-T6	N/A	5×10^{-4} ~5×10^{-3}		
	Copper (pure, annealed)	20 ~ 550	2.5×10^{-3} ~8×10^{-4}	-73	N/A
	Brass	50 ~ 600	3×10^{-3} ~6×10^{-3}	N/A	N/A
	Iron (pure, cold drawn)	0.83	2×10^{-3} ~2×10^{-2}	70	Torsion
	Iron alloy (0.001% C)	1	2×10^{-5} ~6×10^{-5}	N/A	Torsion
	Stainless Steel	N/A	2×10^{-3} ~1.5×10^{-2}	N/A	Torsion
	Iron alloy (ALSI 403)	N/A	2×10^{-3} ~7×10^{-2}	N/A	Torsion
	Lead (pure)	20 ~ 160	8×10^{-3} ~1.4×10^{-2}	N/A	Bending
	Magnesium (pure, casting)	60 ~ 400	6×10^{-2} ~1.4×10^{-2}	N/A	Bending
	Nickel (pure, casting)	N/A	1.5×10^{-4} ~4×10^{-3}	N/A	Torsion
	Platinum (pure)	N/A	8×10^{-5}	N/A	N/A
	Silver(annealed)	N/A	5×10^{-6} ~9×10^{-6}	-23	N/A
	Titanium (pure)	0.5	1×10^{-3} ~7×10^{-2}	550	N/A
	Tungsten (pure)	0.1	2.2×10^{-4}	N/A	N/A
	Zinc	1 ~ 5	1.9×10^{-3}	N/A	N/A
Polymer	Nylon	0.001 ~ 100	0.076 ~ 0.048	30	N/A
	Polyethyl Methacrylate	200	0.07	20	Bending
	Polyethylene	12	0.23	60	N/A
	Polyethyl Chloroacrylate	200	0.02	20	N/A
	Polymethyl Methacrylate	0.001 ~ 400	0.021 ~ 0.0196	25	N/A
	Polypropylene	10	0.095	20	N/A
	Polystyrene	0.1	0.019	25	N/A
	Polyvinyl Acetate	500	0.486	10	Torsion
	Rubber (vulcanized)	4000	1.5	All range	N/A
	Rubber (gum stock)	0.1 ~ 1	0.15 ~ 0.43	20	N/A

As stated above, this research requires high stiffness and high damping properties. Lakes depicted the relation between stiffness and damping capability, tan δ, for various materials as shown by Figure 7 [19]. The best performance can be on upper right corner that has stiffness like structural metals and damping like rubber. This research's target is tan δ larger than 1.0.

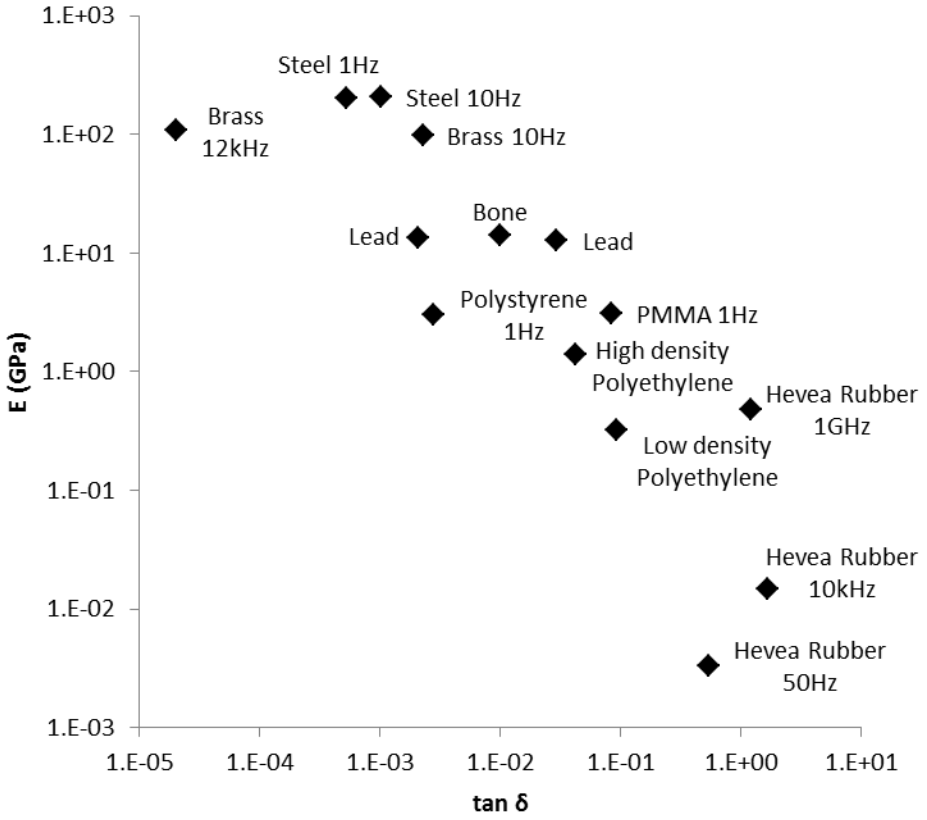

Figure 7. Stiffness-loss map (redrawn from [19]). X and y axes designate elastic modulus and tan δ, respectively. Conventional isotropic metal materials exhibit high stiffness but low damping and polymers vice versa.

2.2.2 Elastomer

Elastomers are viscoelasticity polymers that have low elastic modulus and high yield strain generally. The covalent cross-linkages make the elastomer restore its original shape when the tensile stress is removed. Because they are extremely elastic, elastomers can be reversibly stretched up to 700%. [15] Several elastomers' tan δ were measured for preliminary tests. Por-A-Mold S111 (PAM S111) is a two-part polyurethane molding

system and mixed one-to-one by volume and cures at room temperature. This elastomer is commonly used for molds with containing moderately deep undercuts. We poured S111 and cured it into 31.3mm diameter, 26mm high mold as shown in left in Figure 8. The Aerospace Corporation performed cyclic tests on the specimens with 2% strain at 0.1, 0.5, 1.0, 5.0, and 10.0 Hz. They ran 100 cycles at each frequency. Freeman 1040 is also a mold making polyurethane elastomer that shows low viscosity and high tear strength. We cast this elastomer into the same mold as S111 as shown in right in Figure 8, and had The Aerospace Corporation perform the same tests. Figure 9 shows damping for S111 and 1040. Both exhibit the same damping at 0.1 Hz, but S111's damping increases with increasing frequencies. The 1040 is relatively flat across the frequencies.

Figure 8. Por-A-Mold S111, left, and Freeman 1040, right, damping sample specimens were tested from 0.1 to 10 Hz with 2% strain.

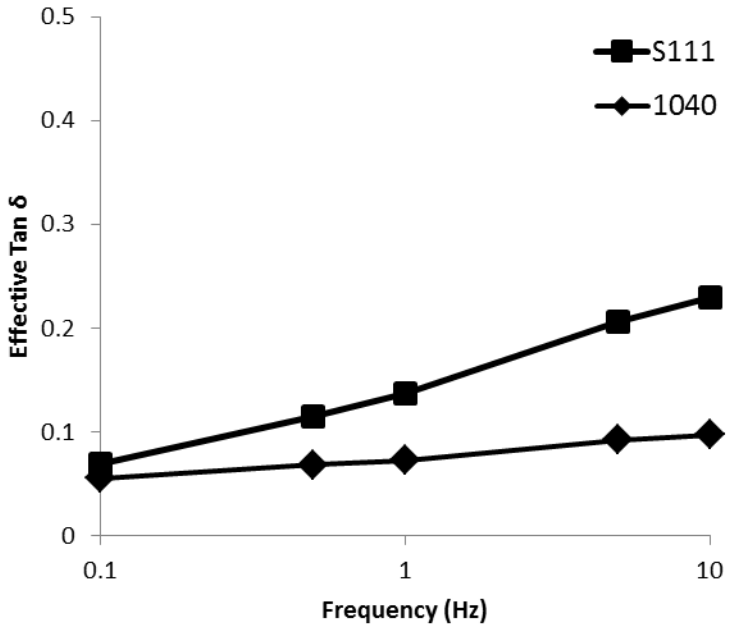

Figure 9. The plot shows that damping, on the y axis, changes across the frequency range (x axis) from 0.1 to 10 Hz. S111's damping, tan δ shows ascending trend and higher damping than 1040's one.

2.2.3 Fluids for Viscoelastic Damping

This research used three fluids: one Newtonian fluid and two shear thinning fluids. Figure 10 shows the fluids' characteristics that change their viscosity by shear strain rate. Newtonian fluid is a simple viscous fluid with a fixed viscosity at any shear rate, but shear thinning and thickening fluids decrease and increase their viscosities, respectively, as shear strain rate increases.

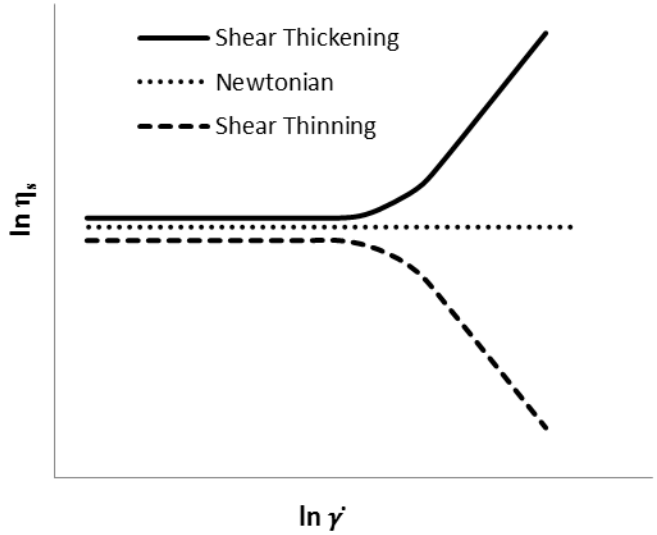

Figure 10. Newtonian fluid does not change its viscosity, η, (y axis) by shear strain rate, $\dot{\gamma}$, (x axis), but shear thinning and thickening flow decreases and increases it viscosity by increasing strain rate (redrawn from [20]).

2.2.4 Other Damping Material using Negative Stiffness Materials

Shaw produced passive vibration isolator by using a bistable composite plate as negative stiffness material. The plate is a 110mm square laid up at [$0°_{3CF}$, $0°_{1S}$, $90°_{3CF}$] The plate supported by its corners incorporates into a dynamic test rig as shown in Figure 11. The outer frame slides on the cart onto the track with little friction and connected to a Shaker. [21]

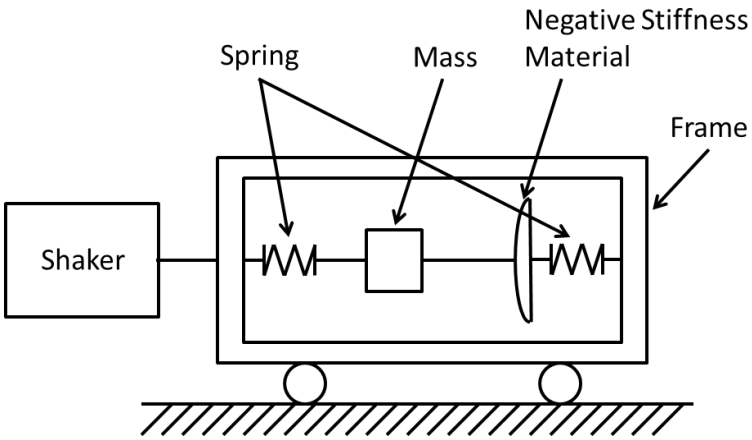

Figure 11. A passive vibration isolator used a bistable composite plate as negative stiffness material (redrawn from [21]).

Platus developed a vertical motion isolator by using negative stiffness mechanism [22]. It has two bars hinged at the center and supported their ends that are free to move horizontally. Opposing force, P, makes this in unstable equilibrium state as shown in Figure 12 (a). Once applying with payload, W, the center pivot point displaces with reaction force, FN, the vertical conventional positive spring displaces with the force, FS, as shown (b) in the fig. The system combined (a) and (b) results stiffness, K = KS - KN, that can approach zero with the weight load, W.

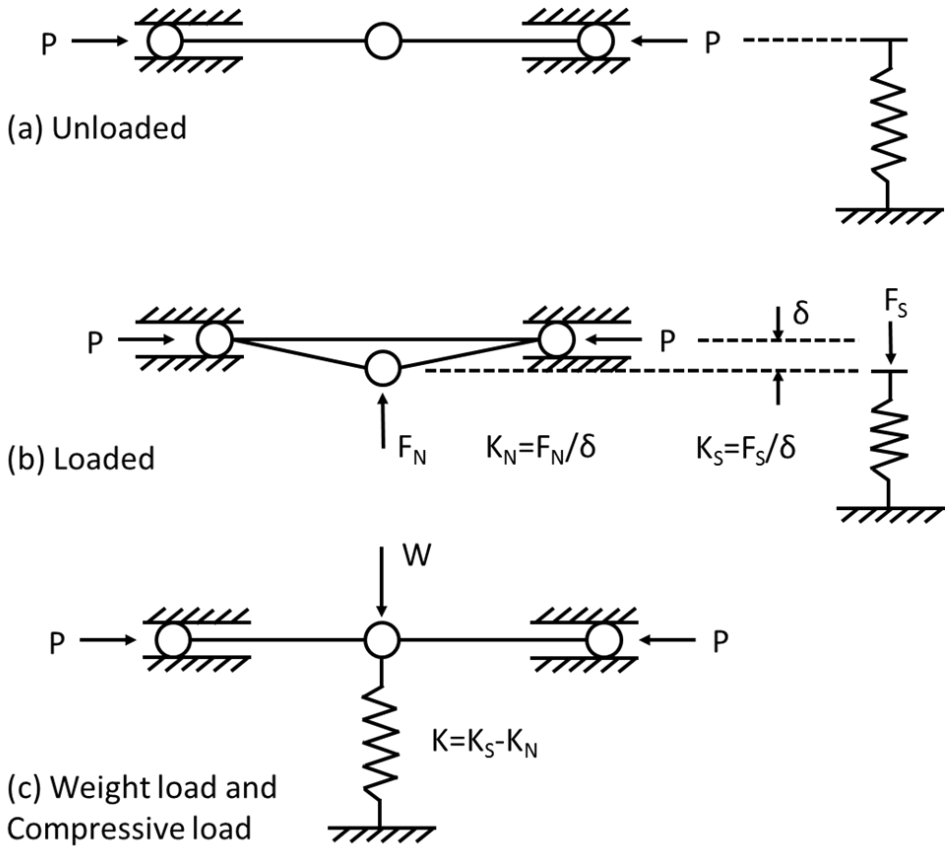

Figure 12. Negative stiffness mechanism isolates the weight load (redrawn from [22]).

2.3 The Machine Augmented Composite Concept

Machine-Augmented Composites (MACs) are tiny structures implanted into a matrix material. The materials can form a composite material that produces specific multiple functions such as shape change and damping. This research suggested a new fluidic damping element.

2.3.1 Previous MAC Research: Z Machine

The Aerospace Corporation developed a multifunctional material called the Z MAC [23]. The machine's cross section shape is like alphabet Z that has sloped double sidewalls. It has a void area in-between the double sloped sidewalls that could be filled with fluids. This machine can be extruded as a pipe in macro scale or fiber in micro scale. Figure 13 describes the Z MAC concept: a stress-conversion machine that converts compressive displacement into shear displacement and vice versa. As shown in image (b), many small solo machines (a) can be embedded in a matrix. The image (c) depicts that applying compressive forces collapses the Z machine and generates shear forces. Conversely, when a shear force is applied on the top, this structure produces a compressive output. The Z machine array infiltrated with air and water damps input loads. [6]

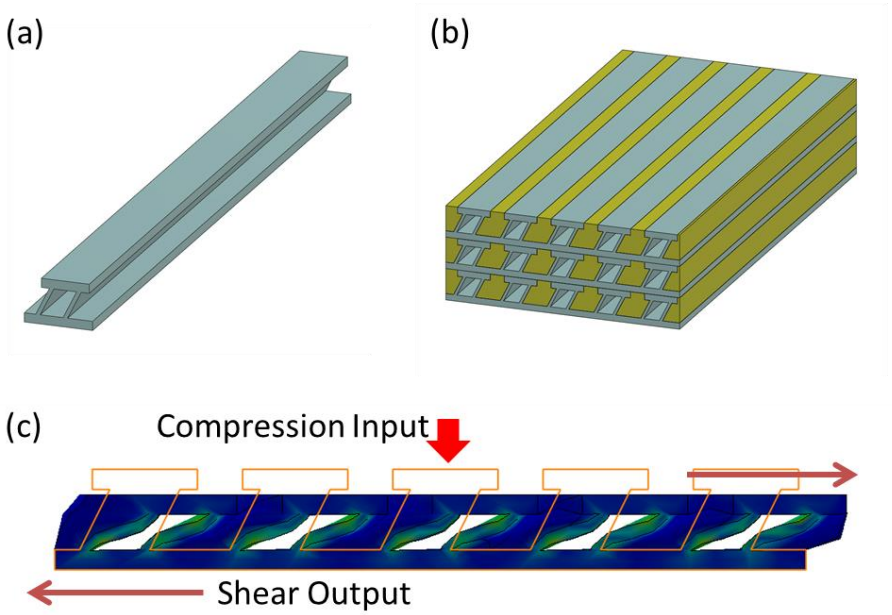

Figure 13. (a) Previous MAC concept, single Z machine, (b) Embedded Z machine in matrix material as a composite structure form, (c) Embedded Z machines' deformation behavior (redrawn from [6]).

2.3.2 Previous MAC Research: HR Machine

Hawkins presented a fluid filled damping machine. It is also an extruded machine that has an hourglass cross section shown in Figure 14. The compressive force from top to bottom moves the pre-buckled sidewalls toward each other and reduces the channel volume. The resulting force on the pre-buckled sidewalls increases pressure and makes a fluid flow in the channel. Tensile force onto the top and bottom on the compressed machine make recover its original shape and pump fluid inside the channel. [6] The fluidic mass transfer and friction onto the sidewalls absorb energy and create damping [16]. This structure can be designed for low frequency applications such as structural

damping for buildings and bridges, or high frequency cases such as launch vehicles or airplanes.

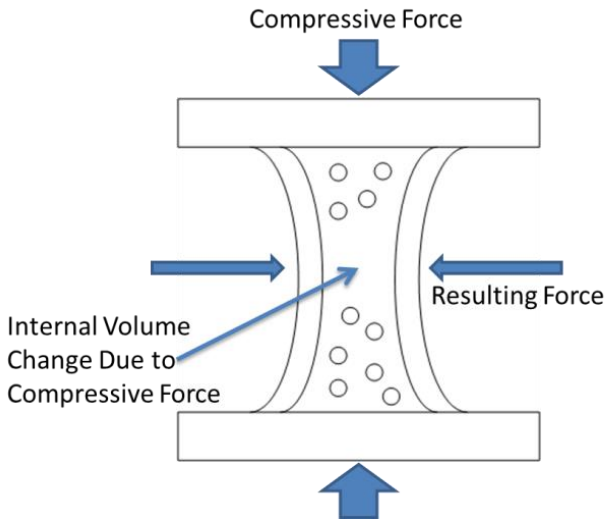

Figure 14. The compressive force from top to bottom can close the pre-buckled sidewalls and reduce the channel volume. This increases pressure and makes a fluid pump through the channel. With tensile forces on top and bottom, the machine recovers its original shape and draws fluid inside the channel (redrawn from [6]).

Kim built the rigid polyurethane hourglass machines shown at left in Figure 15. His experiment used up to 4.7 Pa·s silicone oil, and the results showed that no fluids in that viscosity range improved performance [16]. Figure 16 shows Kim's experimental set up. In the loading phase, the compressive input compresses the HR array and squeezes the fluid out from the channel properly. However, drawing fluid back into the channel as the HG recovers its original shape requires time if the system damps energy well. In that case, the cross head will separate from the array and will not measure the unloading phase damping. McCutcheon's computational study showed that Kim's fluids were not viscous enough. McCutcheon also suggested a design presented at right in

Figure 15 that increase damping. The additional material in the channel decreased hydraulic diameter and decrease pumping volume by 43.41% that would increase the specific damping capacity by 312.3% [24].

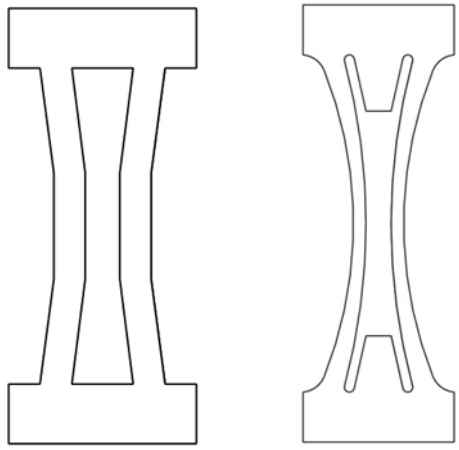

Figure 15. Kim developed the rigid polyurethane hourglass machines at left. McCutcheon suggested additional material that reduces the hydraulic radius and increases the damping capacity as shown on the right (redrawn from [16, 24]).

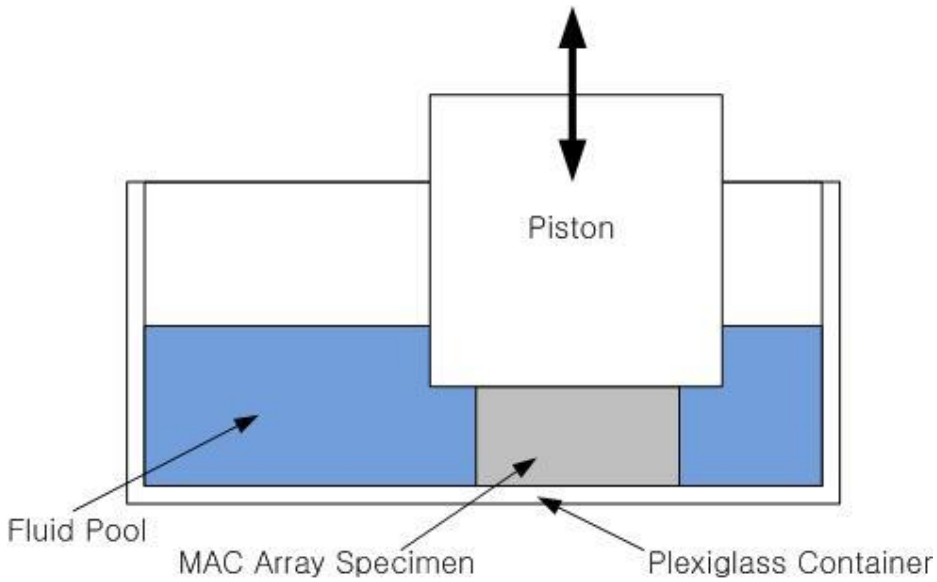

Figure 16. Kim's test set up shows the applied cyclic load has an issue when unloading (redrawn from [16]).

3 EXPERIMENTAL METHODS

3.1 Rapid Prototyping Fabrication

The RP machine manufacturer, Statasys Ltd., supplies P400 ABS material for fabricating. Manufacturer provides properties by producing injection molded ASTM D368 specimens and they report these properties:

- Tensile strength: 22 MPa
- Tensile modulus: 1.63 GPa
- Tensile elongation: 6 %

However, these properties are not produced in RP models because the models are not fully dense. The machine draws the structure layer by layer. The materials will not fuse together and fill the volume completely. That makes voids inside the component. Like fibrous composite materials, orthotropic behavior presents depending on the tool path direction. Figure 17 shows the RP machine's operating software tool paths; odd and even sequence plies have +45 and -45 degree fiber directions, respectively.

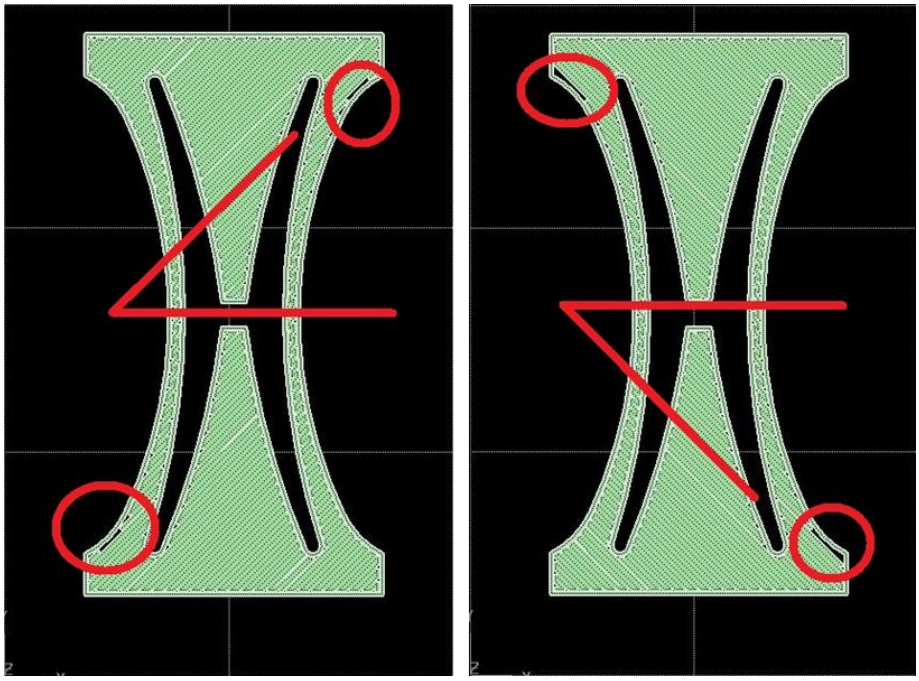

Figure 17. RP machine operating software creates the tool path for an odd sequence ply as shown at left and for an even sequence ply as shown at right.

Because RP machine's resolution is limited, corner areas as highlighted in red circles in Figure 17 are unfilled fully and failed first when we ran a cyclic test at 1Hz for 1000 cycles as depicted in Figure 18. Removing the sharp edge and applying rounding eliminated the void parts and made this structure survive a cyclic test for 1000 cycles. A Solidworks computational model found the homogenized structural elastic modulus that produces the same reaction force as the experiment. The homogenized elastic modulus, 1.5 GPa called the calibrated structural elastic modulus, is less than ABS P400's specified elastic modulus, 1.63 GPa.

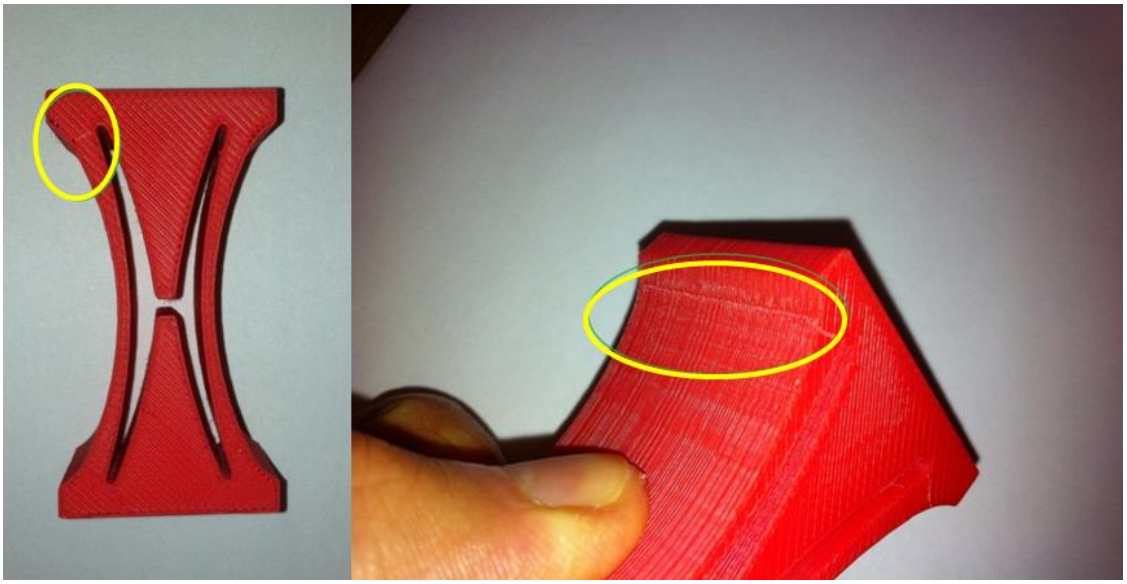

Figure 18. RP machine's coarse resolution caused void area near the sharp edges--highlighted with a yellow circle--and those regions is unsustainable the cyclic test for 1000 cycles.

The Dimension RP machine cannot fabricate our proposed hourglass machine smaller than 64mm high. To produce smaller models, we ordered 64 mm tall models built from Somos 9120 epoxy, a material that shows polypropylene-like properties. Figure 19 presents the Somos 9120 hourglass model. The material properties provided by the Fineline Corp. are

- Tensile strength: 30 - 32 MPa
- Tensile modulus: 1.23 – 1.46 GPa
- Tensile elongation: 15 – 25 %

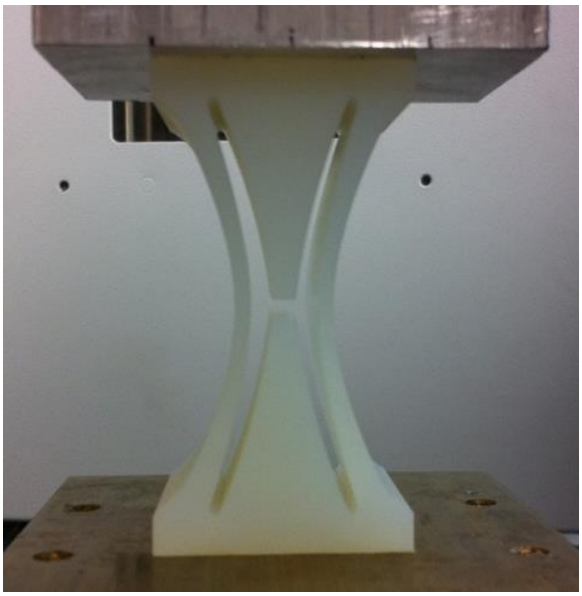

Figure 19. To produce smaller hourglass than 64mm tall, Somos 9120 epoxy material hourglasses were built that shows polypropylene like material properties.

3.1.1 Low Hydraulic Radius HourGlass (LHG)

This research proposes improved hourglass machine design as shown in left picture in Figure 20. The upper and lower triangle shape provides a geometric constraint and lowers hydraulic radius more than previous hourglass machine called as Low hydraulic radius HourGlass (LHG). A 1.25mm displacement or 2% strain on the top surface makes the inner channel gap distance equal throughout the LHG shown in right picture in Figure 20. Two percent strain reduces the internal volume by 42% and forms a uniform gap that keeps most fluid in shear at maximum closure. This hourglass has no sharp corners—as stated above--so it can sustain more than 1000 cycles in compression. The RP machine size limits us to fabricate the LHG with no longer than 170mm. The sidewalls have to have more than two ABS fiber thicknesses to prevent shear buckling.

The smallest size for the hourglass is 64mm height called as 64LHG. We reduced this LHG size into 16mm height called as 16LHG that is made by Somos 9120. It applies 0.3125mm displacement for 2% strain.

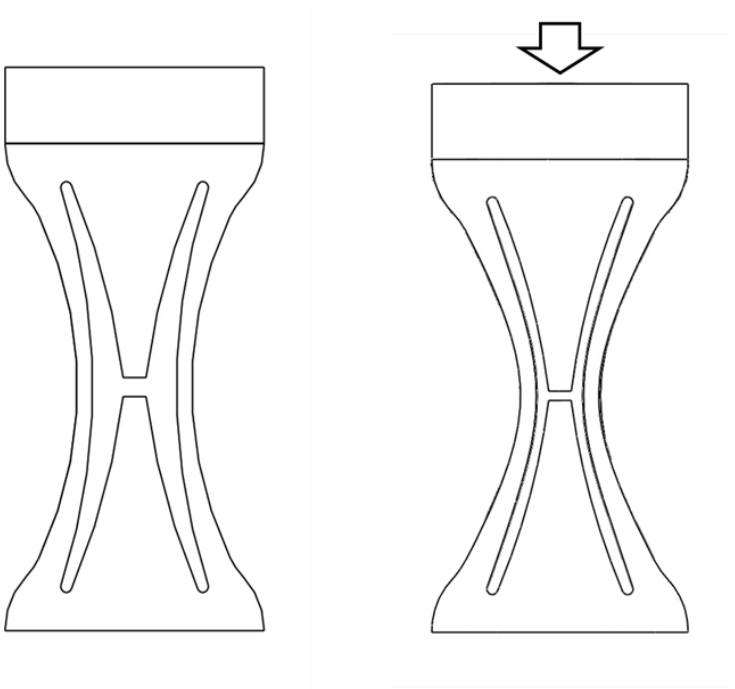

Figure 20. The LHG has upper and lower triangle shape geometric constraints in the channel that lowers hydraulic radius more than previous hourglass machine (left). A 2% strain reduces the internal volume by 42% and forms a uniform gap throughout the LHG's cross section (right).

3.1.2 Low Stiffness HourGlasses (NTG, WTG)

Our research partner, The Aerospace cooperation, suggested new hourglass machine geometries depicted in Figure 21 [25]. These structures reduce stiffness and improve damping. The tan δ is the loss modulus divided by the storage modulus. Decreasing stiffness means reducing the storage modulus in the equation that the tan δ

increases even if the loss modulus remains constant. Baseline LHG has 42.5 MPa structural elastic modulus (1127 N/mm stiffness). Left machine in the figure—called NTG—has a smaller sidewall radius than the baseline LHG that it is more compliant with 32.3 MPa structural elastic modulus (857 N/mm stiffness). The channel volume changes 61% by pumping. The right machine--the WTG—has the smallest sidewall radius and it increases pumping ability, but the structural elastic modulus is as low as 8.97 KPa (0.7N/mm stiffness). The WTG's channel volume changes 15% with 2% strain on the top. The 16LHG made by Somos 9120 has 28.5MPa structural elastic modulus (179 N/mm stiffness) and present small structural damping as shown in the hysteresis loop in the Figure 22 that also presents the structural elastic modulus comparison for all four hourglass machines.

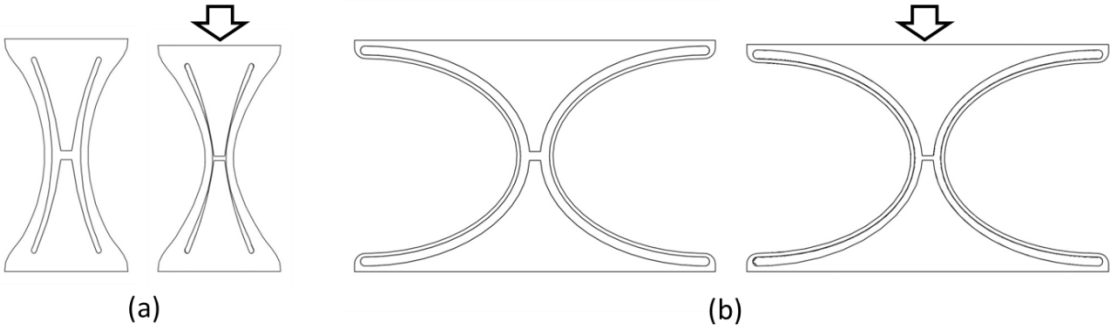

Figure 21. The Aerospace cooperation proposed new hourglass geometries. These new geometries drop stiffness but gain more damping. Left machine called as NTG has smaller sidewall radius than baseline LHG's. Right machine called as WTG has smallest sidewall radius and maximizes pumping ability. [25]

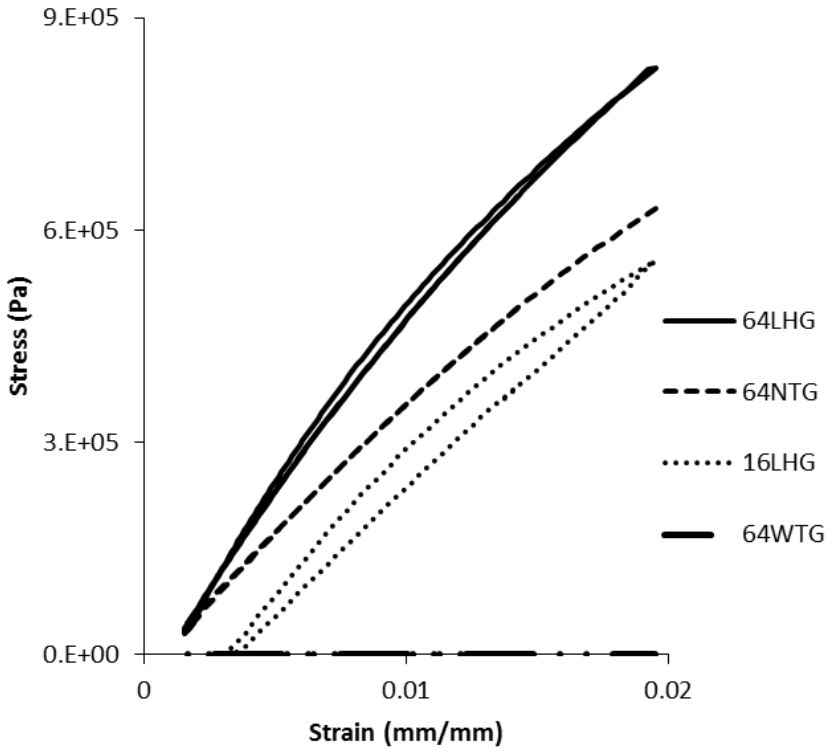

Figure 22. The Aerospace Corp. suggested compliant sidewall hourglasses that increase pumping ability and reduce structural elastic modulus.

3.2 Achieving Adaptive Damping

Common damping systems present high performance at a specific frequency. To achieve passive adaptive damping–good performance across a given frequency range without sensors--we suggest two solutions: stacking LHG layers to create a damping filter and using non-Newtonian fluids within the LHGs.

3.2.1 Stacking Layers for Adaptive Damping

Preliminary test results using highly viscous Newtonian fluid produced larger damping at lower frequency but smaller damping at higher frequency. Observation confirmed the LHG was locked the fluid cannot flow for the high cross head speed. Changing fluid viscosity or scaling the LHG size shifts the peak damping frequency. In a multi-layer LHG, arrays use different viscosity fluids in each layer; each layer will damp well at its target frequency. LHG array stacking is exhibited in Figure 23. The relation between cross-sectional area and dynamic viscosity is shown in equation (8) that is Reynolds number analysis.

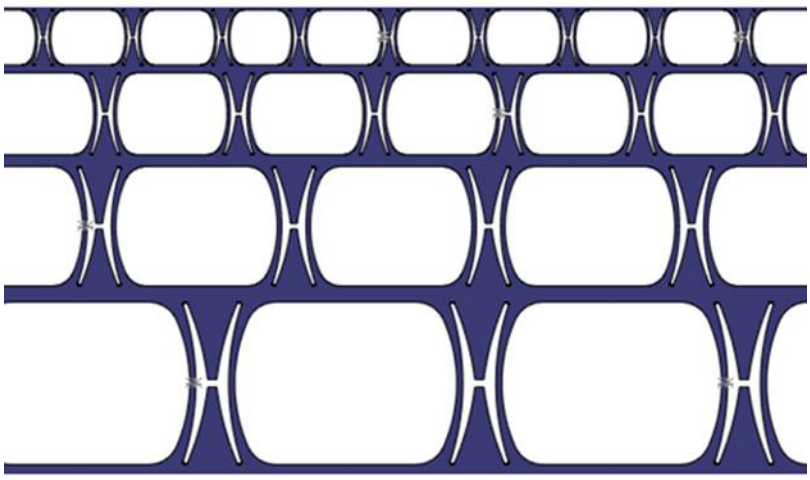

Figure 23. Multi-layer various scaled LHG array stacking with a certain viscous fluid can generate passively adaptive damping through the given frequency regime.

Reynolds number (Re) is a dimensionless number that is inertial forces divided by the viscous forces [26]. The definition includes fluid properties: density, viscosity, velocity, and a characteristic length. A circular pipe's fluid flow generally uses internal

diameter as the length. Non-circular pipes can convert into an equivalent diameter. The standard 64mm tall machine with standard 102 Pa·s viscosity fluid will have the same response as the 16mm tall machine with 22.5 Pa·s viscosity fluid based on the relation shown in equation (8).

$$Re = \frac{\rho V D_H}{\mu} = \frac{V D_H}{\nu} = \frac{Q D_H}{\nu A} \quad \textbf{(8)}$$

where

- D_H is the pipe's hydraulic diameter (m)
- Q is the volumetric flow rate (m^3/s)
- A is the pipe cross-sectional area (m^2)
- V is the mean fluid velocity (m/s)
- μ is the dynamic viscosity (Pa·s)
- ν is the kinematic viscosity (m^2/s)
- ρ is the fluid density (kg/m^3)

We used calibrated silicone oils for the Newtonian fluids with ±1% viscosity value accuracy [27]. Figure 24 depicts its molecular structure. The oils used in this research have 25, 30, 60, and 102 Pa·s viscosities. Silicone oil tends to entrain air—that a disadvantage. When someone pours oil from one place to another, the oil captures air and holds many small air bubbles. [28] A vacuum pump with 15 Torr degased the air bubbles for 48 hours after injecting into the LHG's channels.

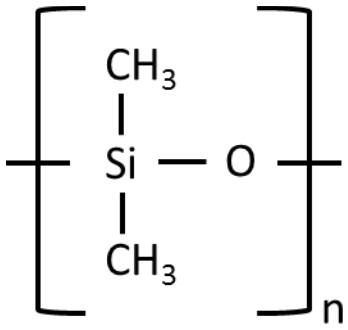

Figure 24. Silicone oils were used for the Newtonian fluid that have 74.15g/mol molecular weight (redrawn from [29]).

3.2.2 Using Non Newtonian Fluids for Adaptive Damping

A LHG array using a non-Newtonian fluid might achieve passive adaptive damping without layering. As shown in Figure 10, the Newtonian fluid does not change its viscosity, η, (y axis) by changing shear strain rate, $\dot{\gamma}$, (x axis). Otherwise, the shear thinning fluid drops its viscosity and shear thickening fluid raises it by increasing shear strain rate. Carboxymethycellulose/water or polyacrylamide/water-glycerin solution can create the shear thinning effects. Polyacrylamide-water solution (PAM) is easy to fabricate and also show similar effect [30]. Figure 25 shows the PAM's molecular structure at left and the shear thinning effect at the right. This study used 5% and 7% PAM in water that produce maximum viscosity.

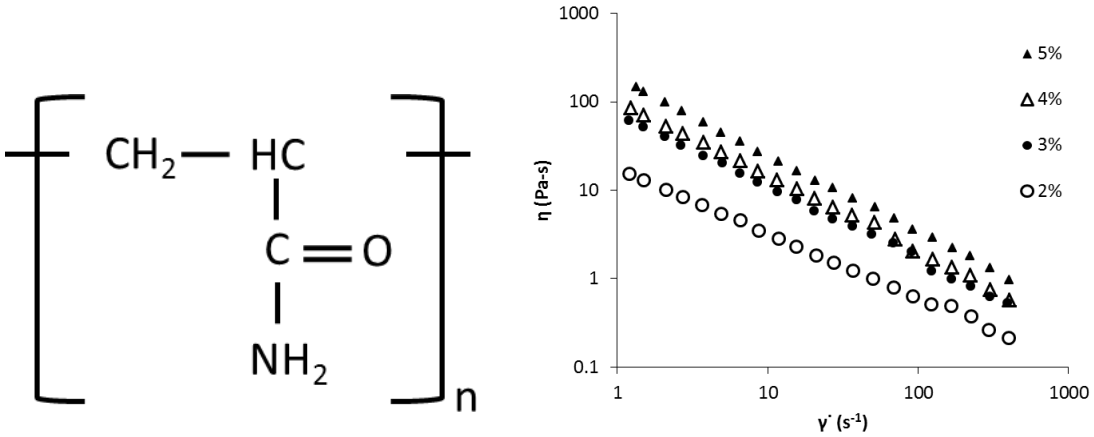

Figure 25. Left depicts the polyacrylamide's molecular structure (redrawn from [31]). The right graph presents the PAM-water solution's shear thinning effect by PAM containing amount (redrawn from [30]).

Another non-Newtonian fluid is shear thickening fluids, Titanium dioxide/sucrose, cornstarch, polyethylene-glycol/water, PMMA/amyl alcohol, and polyisobutylene/polybutene. Lim tested silica particles in the suspending medium polyethylene-glycol (PEG) as presented in Figure 26. Right plot exhibits SiO-PEG's viscosity changes depending on shear stress, and left plot's shear strain rate in its x axis is simply converted from right plot [32]. The viscosity starts to decrease first by increasing strain rate as the shear thinning effect, and then the viscosity increases from a certain point as the shear thickening effect. We fabricated 54% volume fraction SiO-PEG that produces the highest shear thickening effect as shown as the red dashed line overlapped on the Lim's data. The rheology meter met the limitation when our fluid started to show shear thickening effect. The 54vol% SiO-PEG is stable in room temperature, and does not entrain air. Degassing is not required.

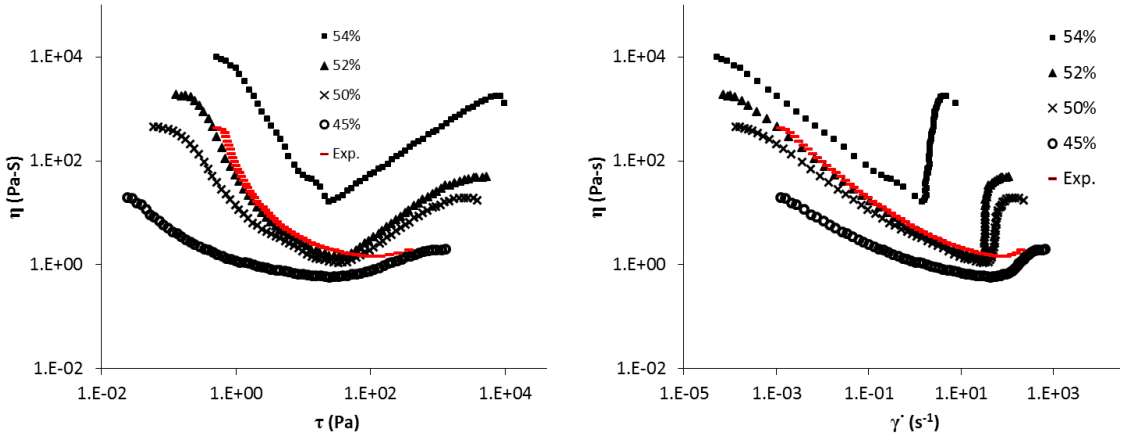

Figure 26. Right plot shows viscosity changes by shear stress. Right plot's x axis is converted from left plot's one. The red dashed line is our 54% volume fraction SiO-PEG data overlapped onto Lim's data (redrawn from [32]).

3.3 Test Set Up

The MTS 810 produced cyclic tests with displacement control. In the first compression phase, the specimen can properly squeeze and pump the fluid, but in the tensile phase, the specimen absorbs energy and the grip displaces faster than the specimen's shape recovery that separates from the specimen. In the second compression phase, the grip hits the specimen that is still recovering its original shape. Red dash line in Figure 27 highlights the separate issue in the hysteresis loop. To prevent this separation, we developed the constraint grip that holds the LHG specimen in both compressive and tensile phases as exhibited in Figure 28. On tensile loading, the specimen might not recover its original shape as fast as the crosshead moves. In that case, the cross head pulls out the specimen by force and open the channel to pump the fluid into the channel.

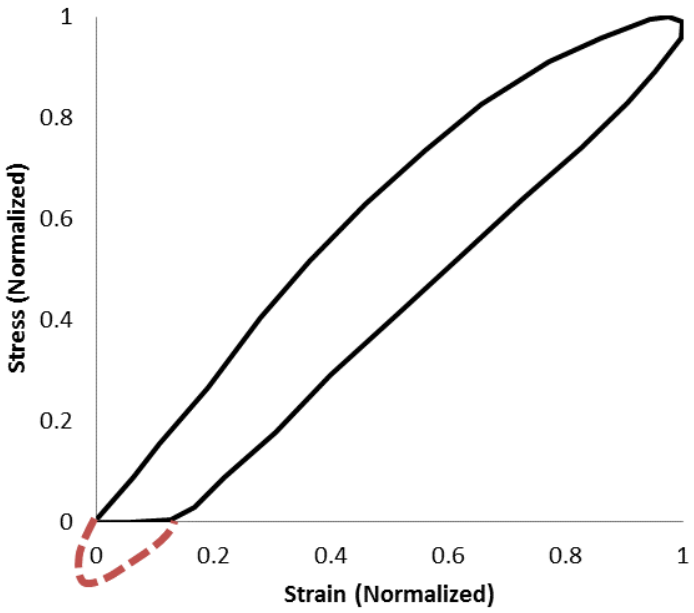

Figure 27. Unconstraint grip separates from the specimen and loses some hysteresis loop area as highlighted as a red dashed line.

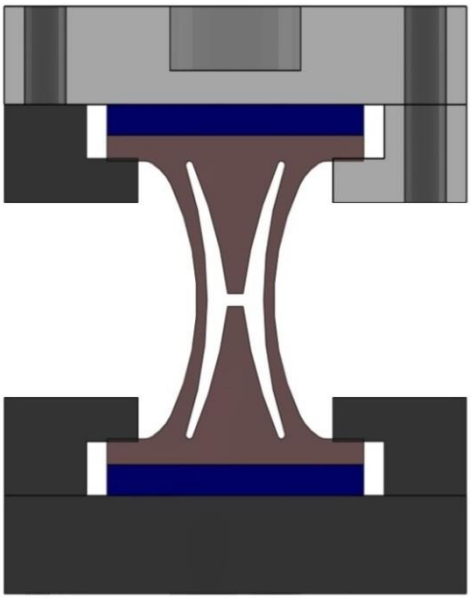

Figure 28. The constraint grip keeps holding the LHG specimen and prevents separation even in high damping and high frequency displacement cases.

The MTS machine applied a cyclic load on the constraint specimen. Figure 29 presents 1 Hz case example that applies three strain conditions:

- Compression/compression (CC) strain: from 0.15% to 2%
- Half Compression/compression (0.5 CC) strain: from 0.07% to 1%
- Compression/tension (CT) one: ±2%

This research carried out the cyclic tests across from 0.1 to 10 Hz, 0.1, 0.2, 0.5, 1, 2, 5, and 10Hz. Ten cycles are sufficient to reach a steady state approximately, and we extracted the tenth cycle and measured the hysteresis loop size.

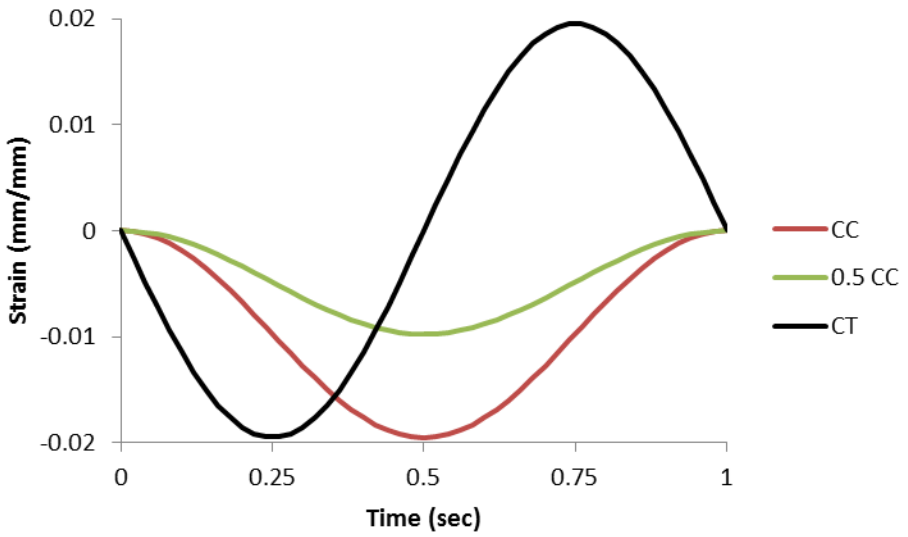

Figure 29. This figure shows the applied strains: compression/compression (CC) with 0.15 ~ 2%, half compression/compression (0.5 CC) with 0.07% ~ 1%, and compression/tension (CT)with ±2% strain.

3.4 Cyclic Test for Solo 64LHG

The baseline 64LHG's cross section geometry is shown in Figure 30 that has 170 mm length. First, a dry test measured the LHG's structural damping without any fluids. Figure 31 exhibits the dry test set up. Second, we filled the channel with silicone oils at 30, 60, and 102 Pa·s and then performed cyclic tests. To contain fluid and make a channel wet, 25mm length reservoirs are attached on the LHG's both ends as depicted in Figure 32. The reservoir ends have transparent windows that we can check the channel closing and fluid level changing. The 5% PAM-water solution and 54 vol% SiO-PEG injected into the channel produced shear thinning effects in cyclic tests.

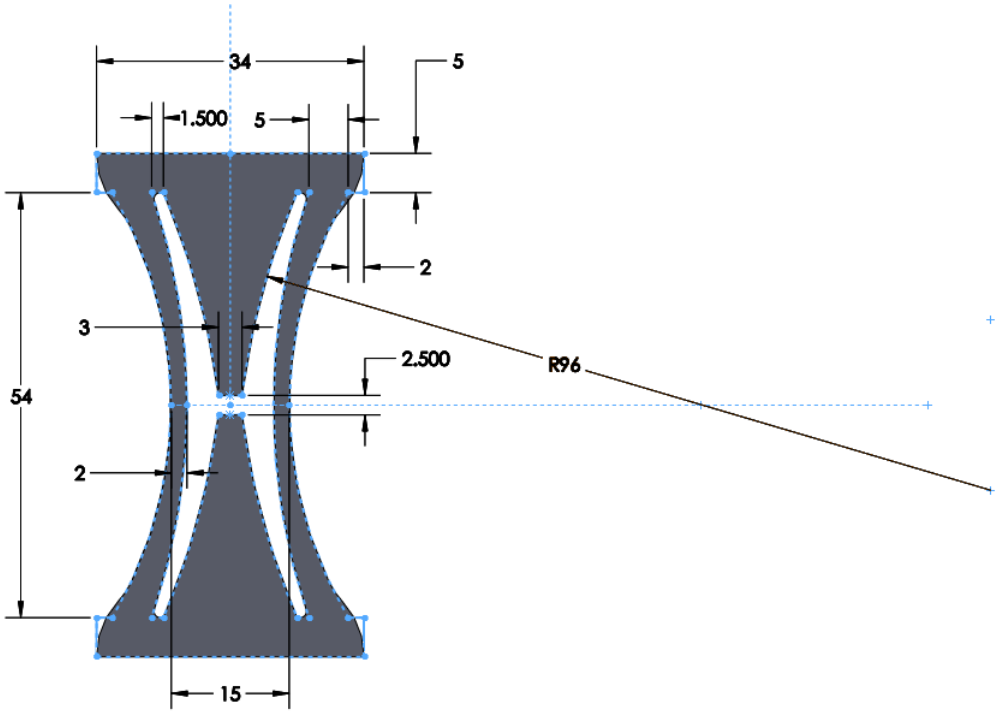

Figure 30. The baseline LHG is called as 64LHG because it is 64mm tall.

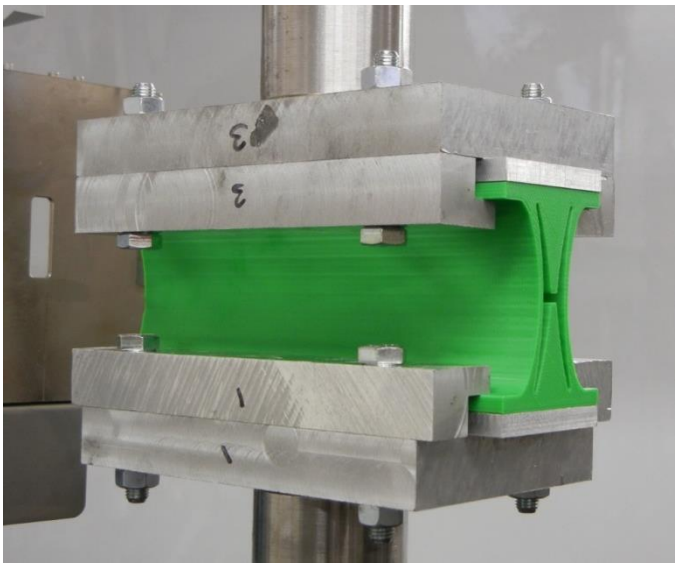

Figure 31. The 64LHG was run dry to measure LHG's structural damping without any fluids.

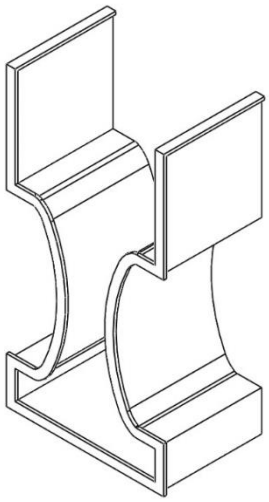

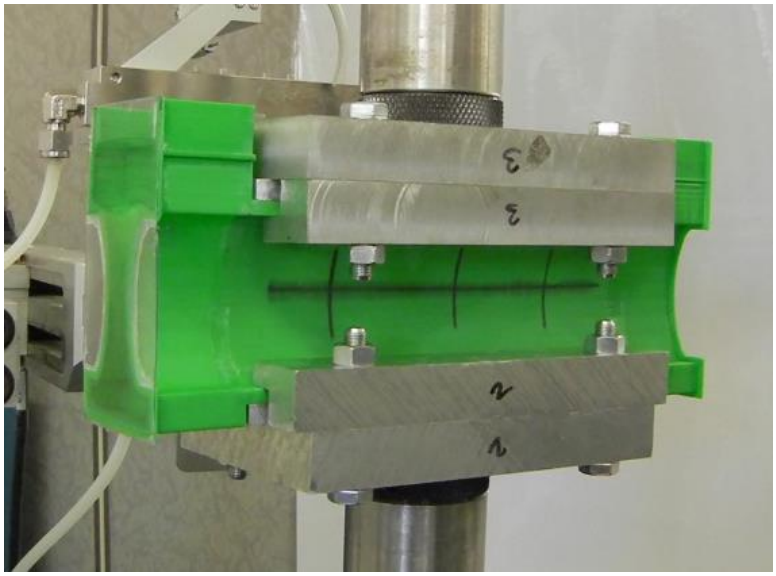

Figure 32. The reservoirs on both ends contain fluid, and windows at the ends allow checking fluid level and channel closing.

3.5 Cyclic Test for Array 16LHG

Five 16LHGs made by Somos 9120 are arrayed onto 6061 aluminum plates and clued with Loctite super glue ultra-gel control. In-between the LHG cells, S111 polyurethane elastomer was injected and cured in it. Four holes were drilled at the ends to constraint the specimen with fixtures Figure 33 shows the panel's shape and dimension.

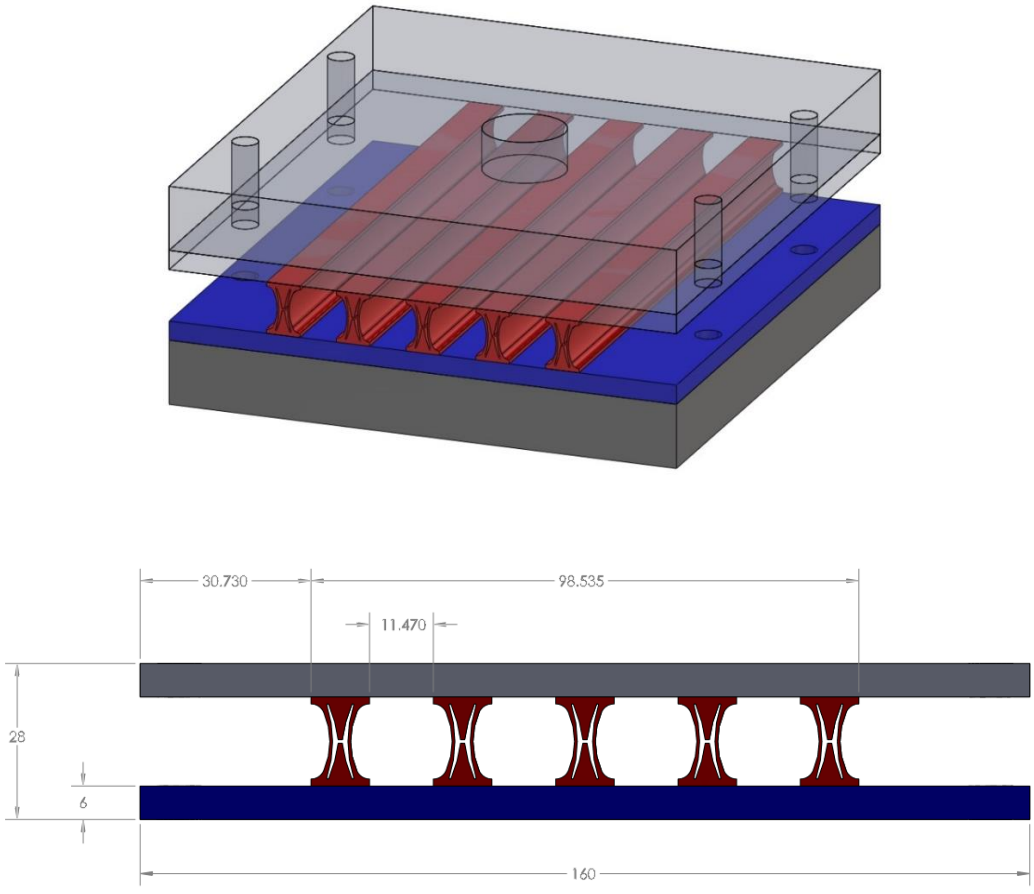

Figure 33. Five 16LHGs, 16mm tall LHG, were arrayed and Polyurethane elastomer, S111, injected in-between the 16LHG cells added performance.

Preliminary experiments showed that elastomer added between LHGs improved damping over elastomer alone even though the hourglasses increased panel stiffness. Left picture in Figure 34 shows an elastomer alone case that the maximum damping occurs at the sides where the shear deformation is greatest. The elastomer near the center is ineffective because the shear deformation is zero. On the other hand, elastomer filled HG arrays put an elastomer into high shear deformation at every hourglass element wall as shown in the right picture.

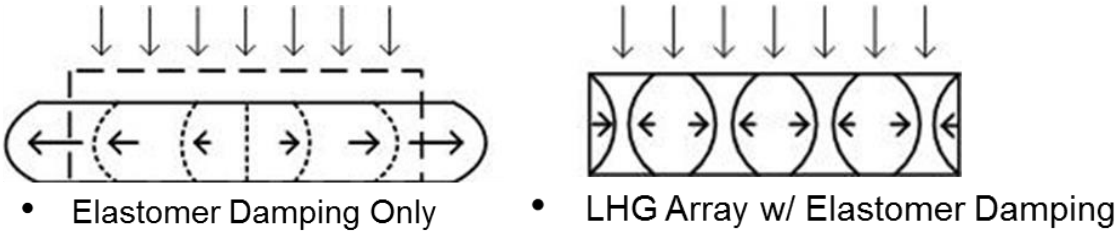

Figure 34. Damping compared between elastomer alone–shown at left—and an HG array filled with elastomer on the right. Unlike neat elastomer, the array damps near every machine sidewall.

To keep the channel wet during cyclic tests, 10mm long reservoir—that did not increase stiffness as an end boundary condition—was attached by soft sealant silicone glue. Figure 35 shows the actual 16LHG panel and constraint test set up for the MTS machine. We tested this panel with 25 Pa·s silicone oil for a simple viscous fluid, and 5 and 7% PAM-water solution for a shear thinning fluid. Cyclic tests with the 54vol% SiO-PEG had technical difficulty because injecting the fluid into the small 16 LHG's channel was challenging.

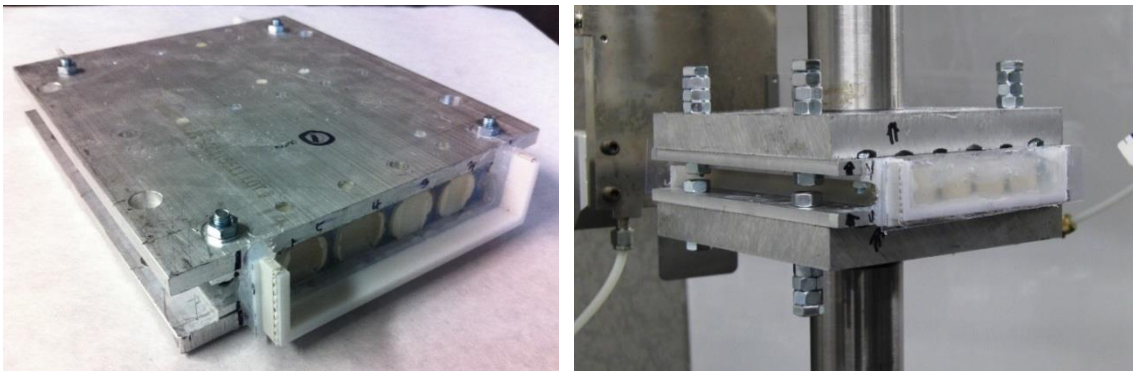

Figure 35. The actual 16LHG array panel at left and the constraint test set up at right.

3.6 Cyclic Test for Solo 64NTG and 64WTG

The 64NTG and 64WTG were built by Dimension RP machine with ABS P400, and tested in the same manner as 64LHG. Figure 36 presents the 64NTG and 64WTG's cross section shapes and dimensions, and both hourglasses have 170mm long. The 64NTG was tested with 60 Pa·s silicone oil. After confirming the trend that reducing structural stiffness increases damping, we moved on the most compliant hourglass case, WTG. The 64WTG was injected by 60 Pa·s silicone oil and 54vol% SiO-PEG for the cyclic tests.

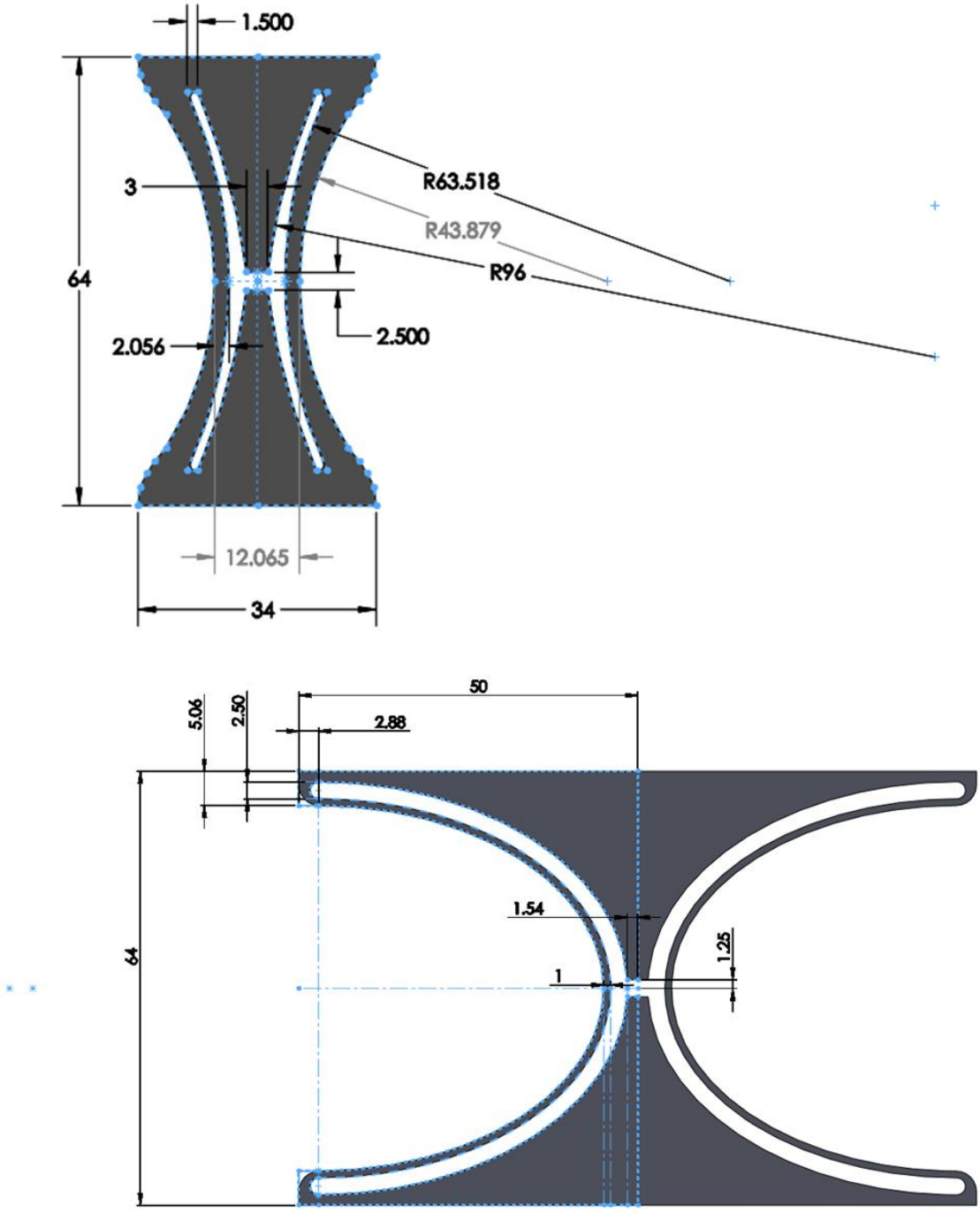

Figure 36. Dimension RP machine produced 64NTG shown in the top image and the 64WTG shown in the bottom image that are 170mm long.

4 EXPERIMENT RESULTS

4.1 Damping for Solo 64LHG

This section describes the solo 64LHG's damping in dry and wet condition. Wet condition sections appear in three parts: simple viscous fluid, PAM-Water solution, and SiO-PEG cases.

4.1.1 Damping in Dry Condition

The 64LHG was tested in dry condition on the constraint fixture, first. This test shows solely 64LHG's structural damping excluding fluidic damping. Figure 37 presents the dry condition cyclic test's hysteresis loop. It shows almost no damping, 0.036 tan δ, and does not change with input frequency.

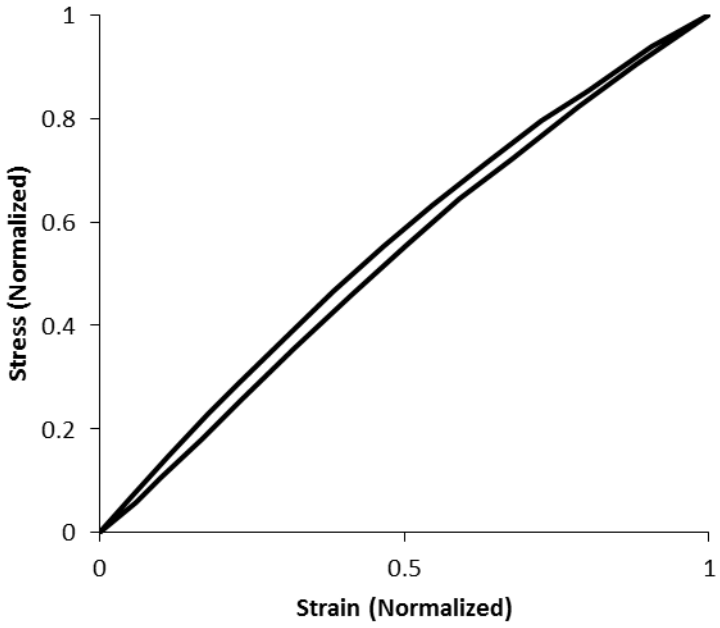

Figure 37. The 64LHG's dry condition cyclic test shows almost no damping.

4.1.2 Damping with Simple Viscous Fluids

High viscous silicone oils were used as Newtonian fluids that have 30, 60, and 102 Pa·s viscosity. The fluid level rises in compression phase and lowers in tensile phase, and we can observe the changes through the windows attached the reservoir's ends. The compression/compression (CC) and compression/tension (CT) cases' fluid level changes are highlighted as red lines in Figure 38 on left and right images, respectively. Because CT case's displacement is two times larger than CC case's one, the CT case's channel more opens and pumps more fluid than CC case.

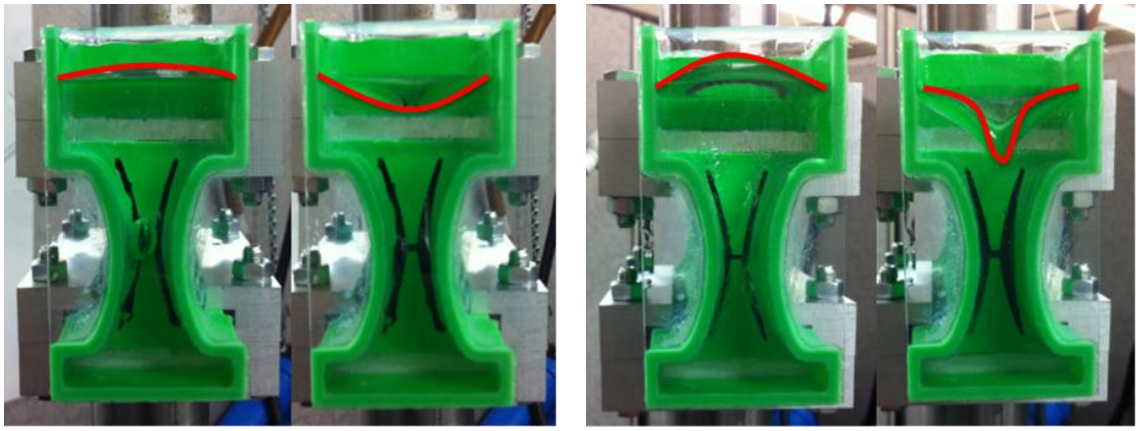

Figure 38. CC case in the left image pair and CT case in the right image pair show fluid level extremes during cyclic tests. The red lines highlight the fluid's free surface.

Figure 39 depicts cyclic test results in each viscosity fluid case. The x axis designates applied frequency in log scale, and the y axis presents the damping, tan δ. From top to bottom, 30, 60, and 102 Pa·s viscosity silicone oil cases are shown. Left and right column data are CC and CT cases' plots, respectively. In using 30 Pa·s silicone oil case, the peak damping occurs between 0.5 and 1Hz. In the same manner, the peaks show between 0.2 and 0.5Hz for 60kcP oil and between 0.1 and 0.2Hz for 102kcP oil. The peak shifts from left to right by reducing the fluid viscosity. The CT case shows similar peak shifting phenomenon to CC case, but lower performance. Even though CT case opens the channel widely and pumps more fluid, the CT case's stiffness is about 17% higher than CC case's. The tan δ is defined as loss modulus divided by storage modulus. This larger stiffness increases the tan δ's denominator, storage modulus that is the damping is lower than CC case as a result.

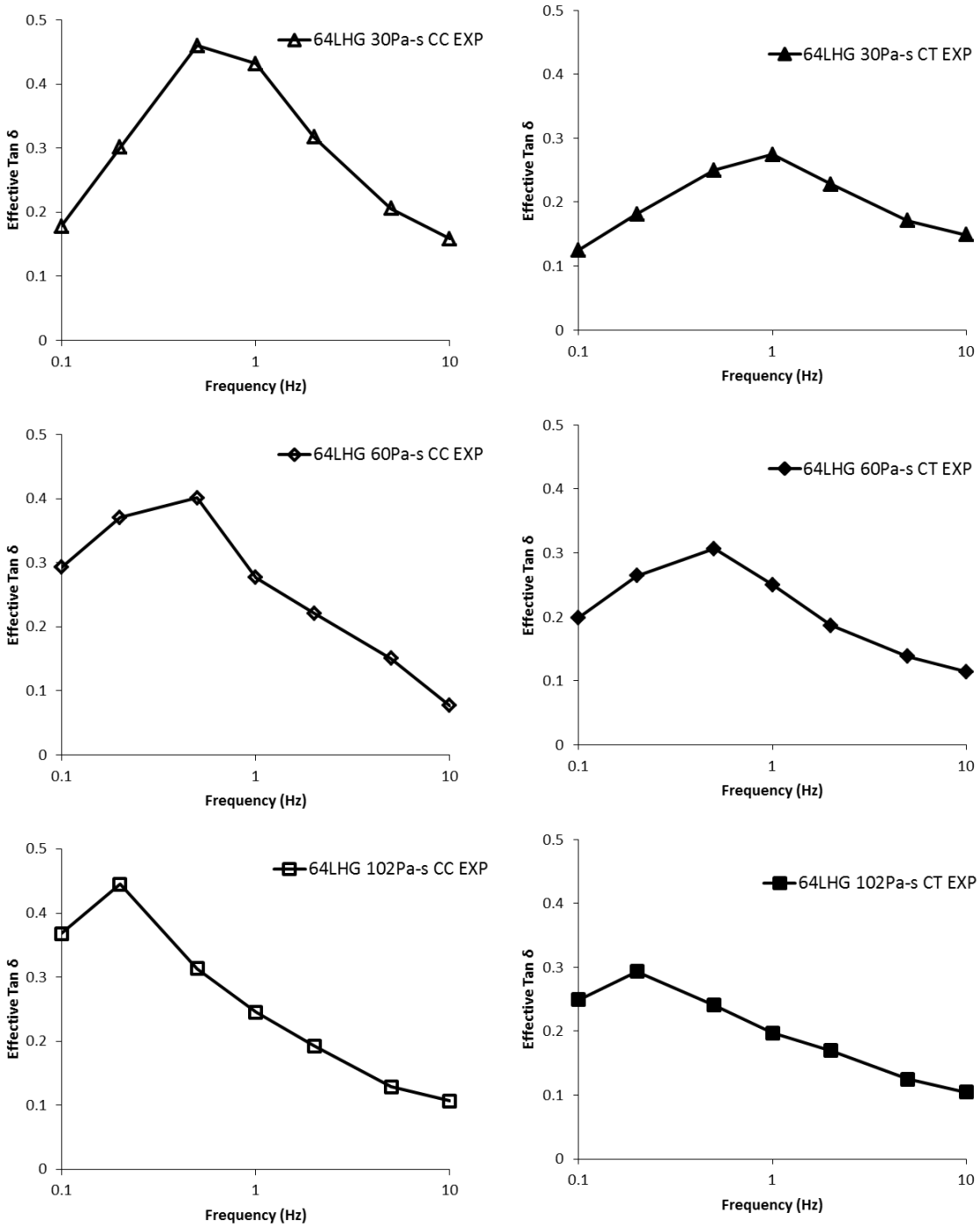

Figure 39. High viscous silicone oils at 30, 60, and 102 Pa·s--from top to bottom--were used as Newtonian fluids. The CC case damping in the left column is higher than the CT case in the right column.

4.1.3 Damping with PAM-Water Solution

The 5% PAM-Water solution showed shear thinning effects as depicted in Figure 25 can work within the 64LHG channel. The fluid's characteristic changes with changing input frequencies. In low frequency such as 0.1Hz, the fluid's viscosity is as high as maximum that makes the LHG will show good damping. The viscosity can decrease in high frequency case such as 10Hz, and the fluid flows well in the channel that produces also a good damping. The PAM-Water solution dries and changes its properties in short time. Air pressured syringe forced the fluid into the channel quickly. Figure 40 depicts the 64LHG with 5% PAM-Water solution. This fluid with the baseline 64LHG produces good adaptive damping from 0.1 to 10 Hz that means a relatively flat line as presented in Figure 41, but the damping is not high enough to meet the requirement. Scaling down the LHG would solve this issue as described in section 4.2.1.

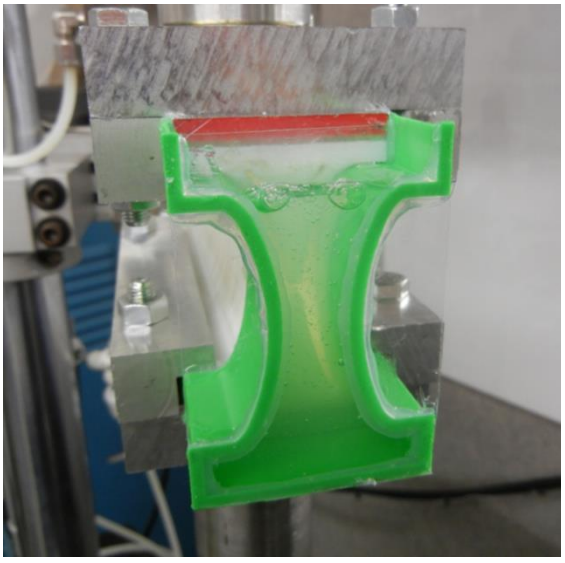

Figure 40. The 5% PAM-Water that shows a shear thinning effect works with 64LHG.

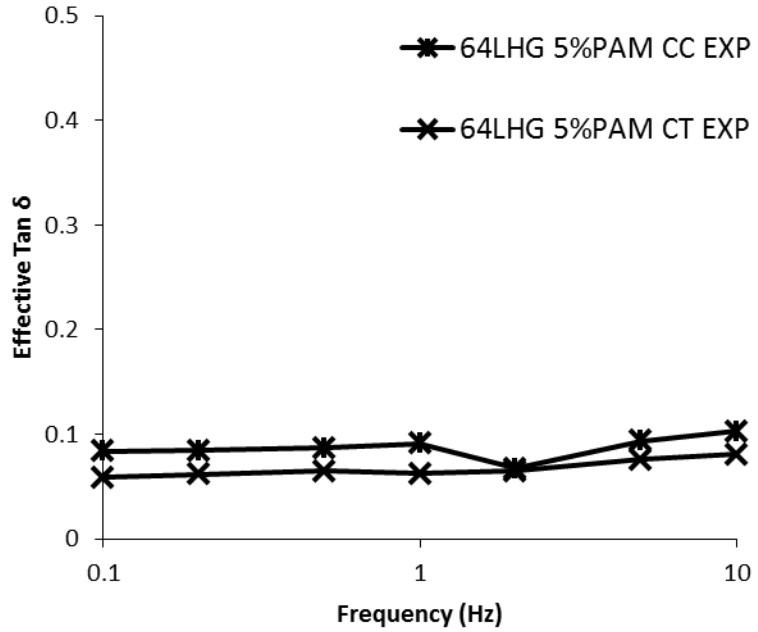

Figure 41. The 5% PAM-Water solution in the 64LHG channel produces good adaptive damping, that is, a flat region, across the frequency range.

4.1.4 Damping with SiO-PEG

The SiO-PEG is a shear thickening fluid, but it produces the shear thinning effect as shown in Figure 26. Figure 42 displays fluid level change by pumping this fluid. The fluid's top surface in the reservoir did not show concave/convex shape changes like the silicone oil because the fluid changes its viscosity. In low frequency cyclic test, the fluid's viscosity drops too fast to work in low frequency range for the 64LHG. As shown on the plot in Figure 43, the 64LHG with SiO-PEG does not show good damping from 0.1 to 1 Hz for both C/C and 0.5C/T cases, and increases tan δ from 1 Hz point.

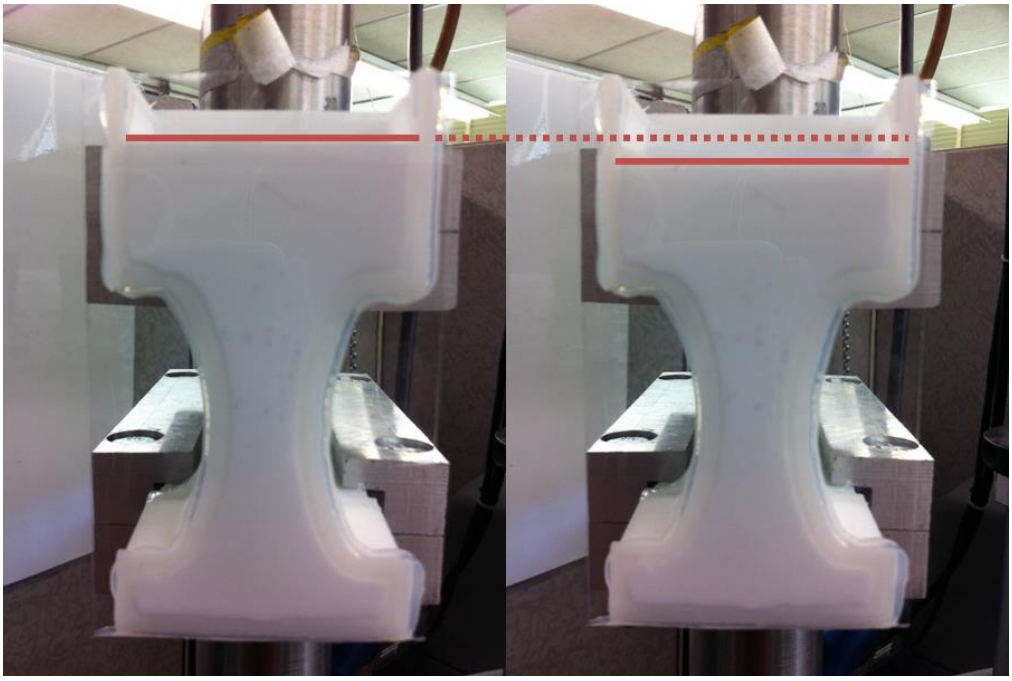

Figure 42. The 64LHG with 54vol% SiO-PEG fluid was tested in constraint C/C and 0.5C/T. Fluid top surface showed flat surfaces in fluid level changing because the fluid's viscosity is adaptive.

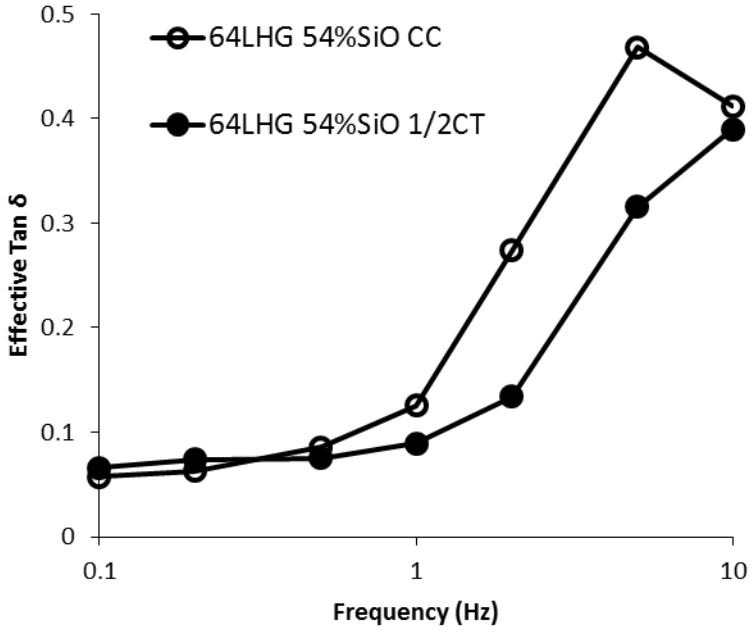

Figure 43. The SiO-PEG's viscosity is too high for the 64LHG in low frequency cases. The tan δ starts to increase from 1 Hz for both C/C and 0.5C/T.

4.2 Damping for Array 16LHG

To produce high adaptive damping, the 64LHG was scaling down to the quarter size, 16mm tall, but the length kept 170mm long. Loctite super glue ultra-gel control glued five 16LHGs onto the Al6061 plates, and S111 polyurethane elastomer filling between the LHG cells helps add damping. Solo and double stacked arrays were tested in the constraint condition, the solo 16LHG array panel with 5% PAM-Water solution and a double stacked array with one for 25Pa·s silicone oil wet and the other one for 7%PAM-Water solution wet.

4.2.1 Damping with PAM-Water Solution

Because the PAM-Water solution is highly viscous, an automotive grease pump attached with syringe needle injected the fluid into the 16LHG's narrow channel. Figure 44 exhibits the 16LHG with S111 filling array with 5%PAM-Water solution. We can check the fluid's level changing through the reservoir windows. Figure 45 presents both C/C and C/T strain conditions' cyclic test results. The peak damping occurred at around 0.2 Hz on both cases. Unlike C/C case, C/T strain case showed adaptive damping in 0.32 and 0.38 tan δ range.

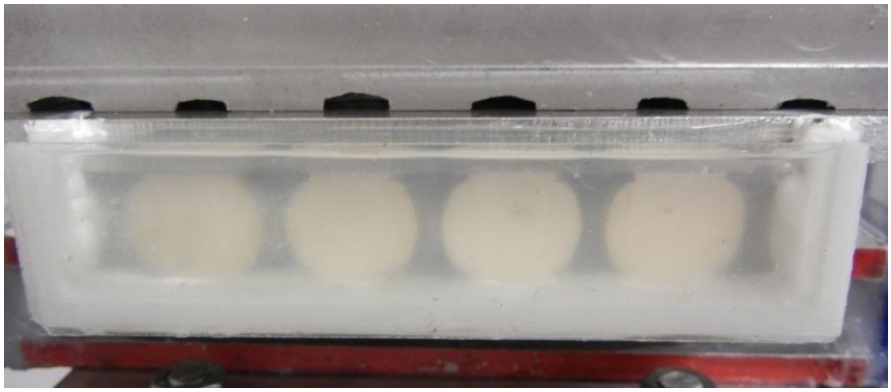

Figure 44. An automotive grease pump injected 5%PAM-Water into the 16LHG's narrow channel.

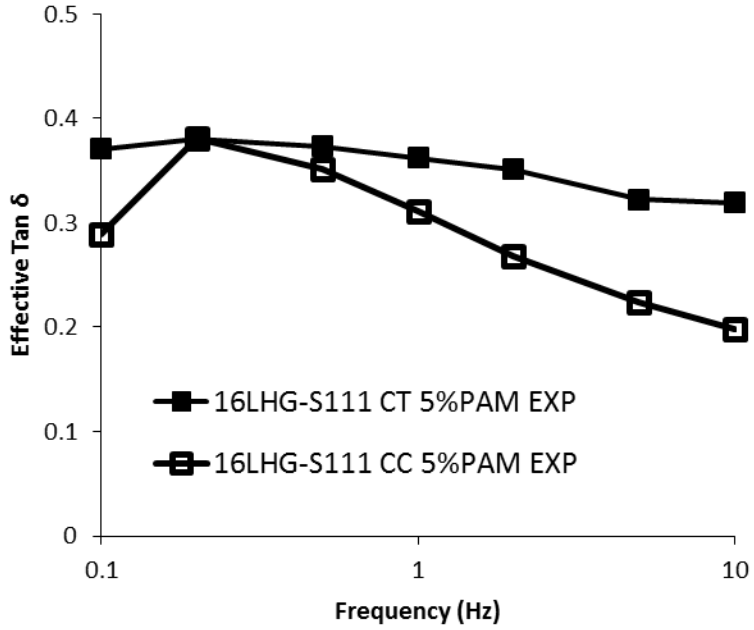

Figure 45. Two strain cases, C/C and C/T, were applied on the 16LHG array. The C/T strain case showed adaptive damping in-between 0.32 and 0.38 tan δ range.

4.2.2 Stacking 16LHG Panels

Two arrays stacked together to increase damping. The 7%PAM-Water solution wet array and 25 Pa·s silicone oil wet array glued together with Loctite super glue ultra-

gel control. Because the two arrays delaminated, we applied C/C case only. Figure 46 and Figure 47 present the stacked arrays' test set up and the cyclic test results, respectively. Because the 25 Pa·s silicone oil wet 16LHG array showed simple viscoelastic damping, it did not produce adaptive damping but added damping with slope as shown in the result. This system has the peaking damping lower than 0.1 Hz. Just like 64LHG, CC case shows a little more damping than half CT case. The tensile phase added higher structural stiffness that is the increasing tan δ's denominator.

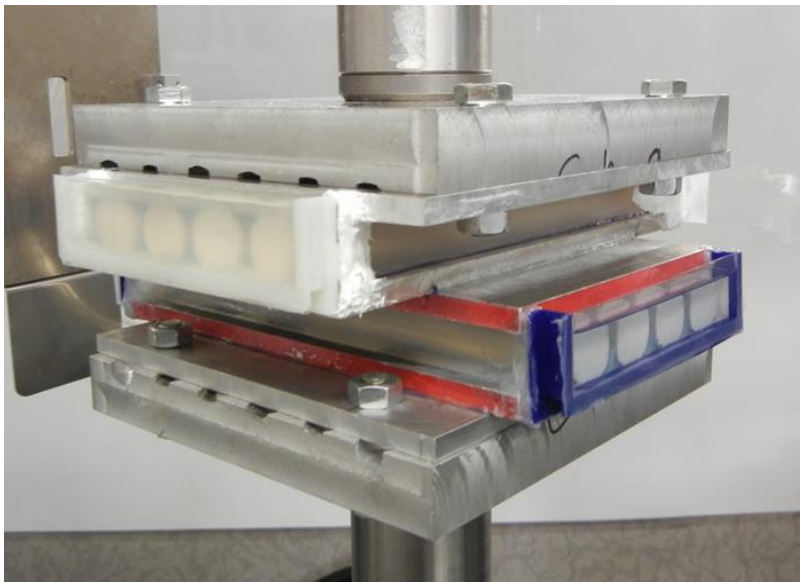

Figure 46. The 7%PAM-Water solution wet array and 25 Pa·s silicone oil wet array glued together and tested in the constraint C/C condition.

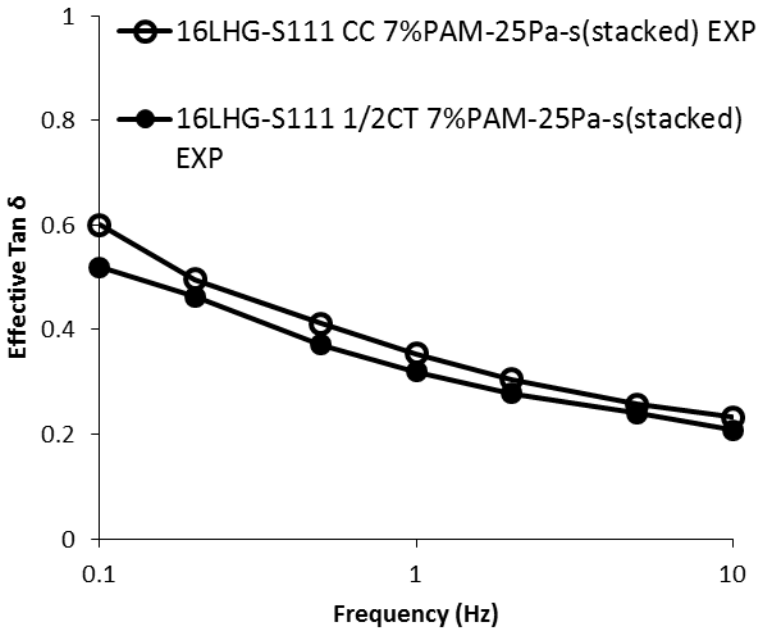

Figure 47. Because the 25 Pa·s silicone oil is a simple fluid, this stacked system did not show adaptive damping, but supplemented viscoelastic damping in lower frequency strain input case on both CC and 1/2CT. Note: the y axis maximum value is one tan δ.

4.3 Damping for Solo 64NTG

The 64NTG has smaller radius on its sidewalls that make the structure more compliant than baseline 64LHG. Changing sidewall shape reduces pumping volume. The undeformed 64LHG's channel volume is 51.72ml and reduced by 29.87ml in the deformed channel that is 42% different. The NTG's channel volume changes from 32.59ml to 19.96ml, 61%. We tested 64NTG with 60 Pa·s silicone oil in the constraint C/C condition. Figure 48 exhibits the fluid level changes by pumping, and the change is less than 64LHG's C/C case because the pumping volume is smaller Figure 49 presents damping results across the frequency range. Compared with 64LHG, the peak damping

occurs in the lower frequency and the tan δ_{eff} is increased. After confirming that reducing structural stiffness helps increase the damping, we moved to test 64WTG that has even more compliant sidewalls and shows maximum damping.

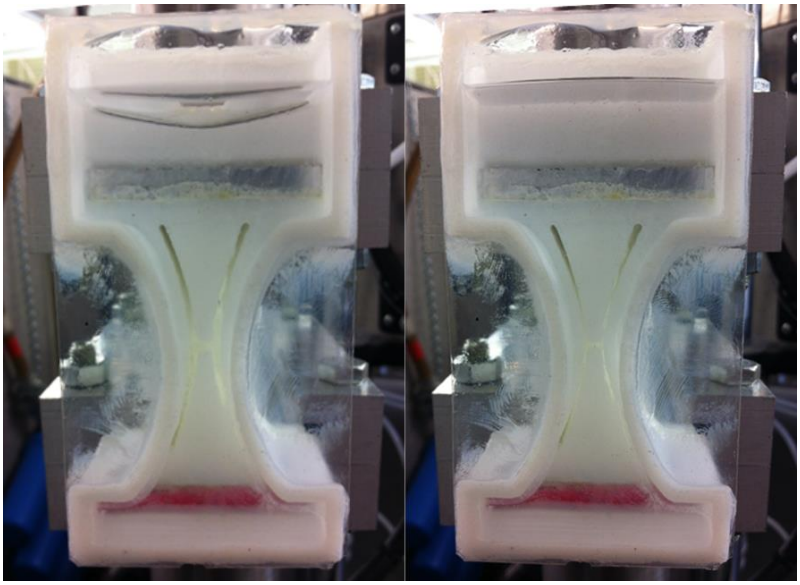

Figure 48. The 64NTG C/C case's fluid level change is less than 64LHG C/C case's.

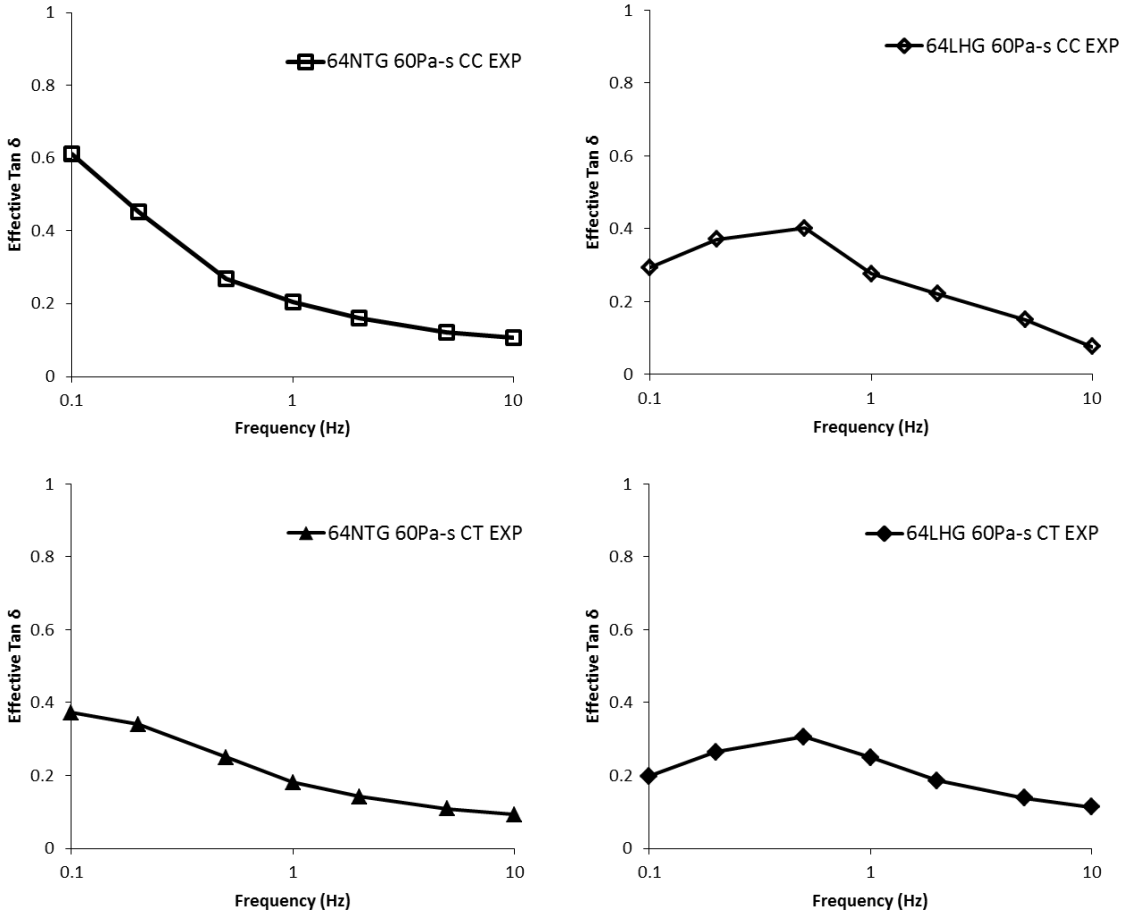

Figure 49. Compared with 64LHG, the 64NTG's peak damping occurs in the lower frequency and the tan δ_{eff} is increased. Left column plots are for the 64NTG's CC and CT cases from the top. Right column plots are 64LHG CC cases' damping data for comparison. Note: the y axis maximum value is one tan δ.

4.4 Damping for Solo 64WTG

After verifying that reducing stiffness increases damping by 64NTG case, we tested 64WTG that shows maximum damping. The 64WTG's channel volume is 593.38 ml and reduced in 504.8 ml by compression that is 15% difference. Two cases were

tested that used two different working fluids, 60Pa·s silicone oil and 54vol% SiO-PEG, injected into the channels.

4.4.1 Damping with Simple Viscous Fluids

The 25mm length reservoir attached on the both 64WTG ends keeps the channel wet during cyclic tests. Figure 50 shows the 64WTG with 60 Pa·s silicone oil test set up. Because the pumping ratio is only 15%, the fluid level change cannot be directly observed, but the performance—as shown in Figure 51—is significantly increased by reducing the structural stiffness from LHG's 1127 N/mm to WTG's 0.7 N/mm.

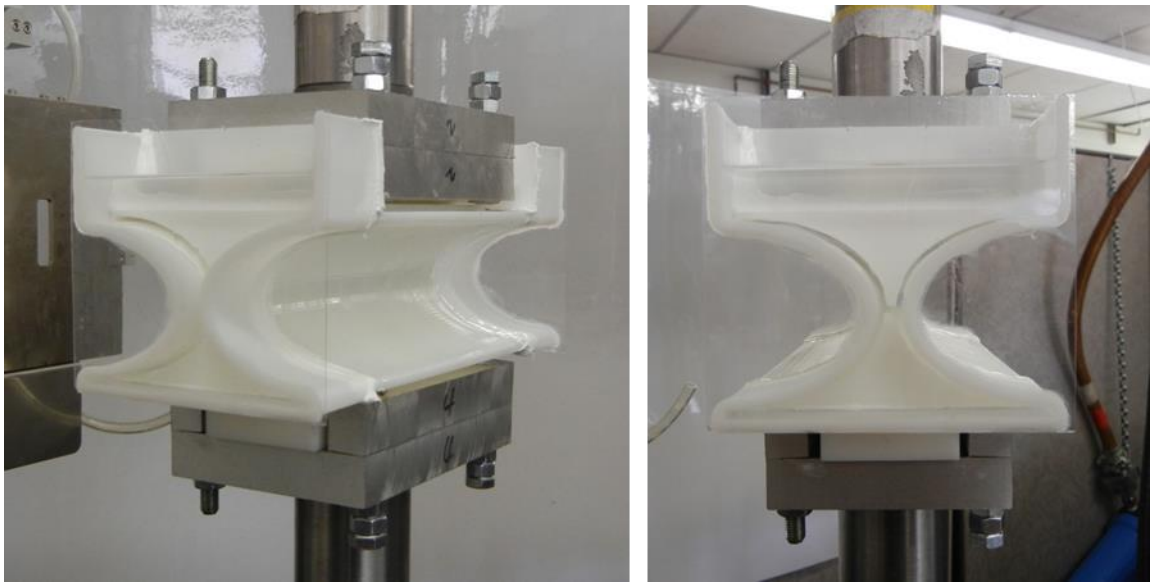

Figure 50. The 64WTG was tested with 60 Pa·s silicone oil.

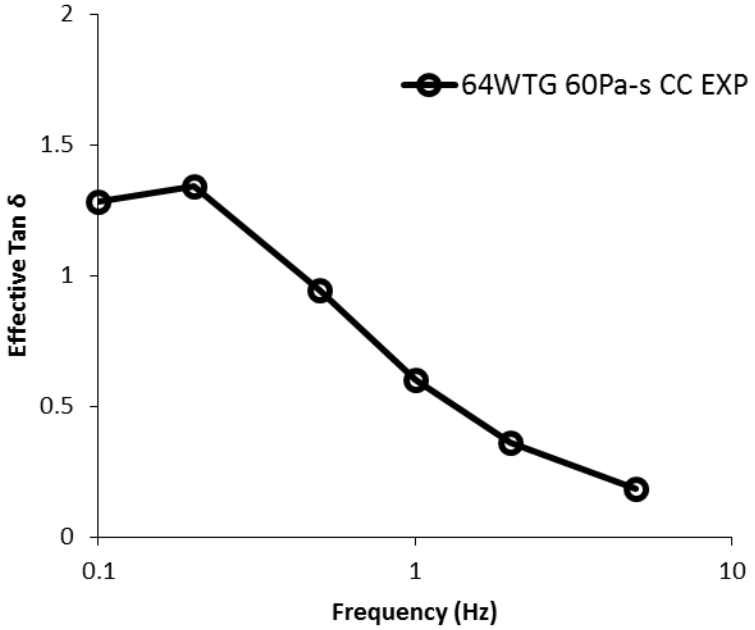

Figure 51. Reducing structural stiffness significantly increases damping in low frequency. Note: the y axis maximum value is 2 tan δ.

4.4.2 Damping with SiO-PEG

The 54vol% SiO-PEG worked in the 64WTG channel as exhibited in Figure 52. The fluid flows well for all across the frequency that the fluid adapts its viscosity in each case. For all three strain cases, C/C, 0.5C/T, and C/T, the damping shows around one or more tan δ and also present flat region for the adaptive damping. Figure 53 exhibits the 64WTG with 54vol% SiO-PEG in all three strain cases.

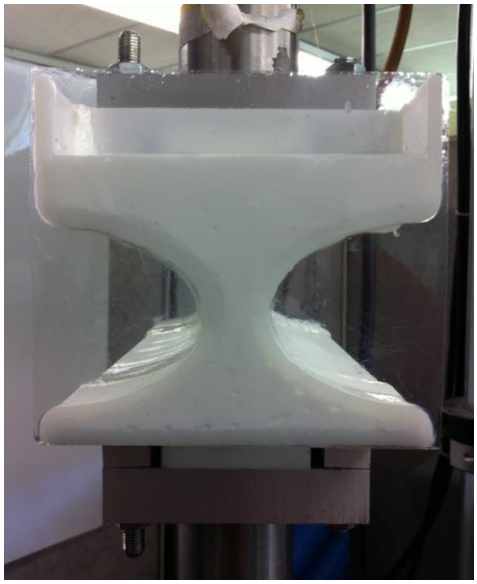

Figure 52. The 54vol% SiO-PEG worked with the 64WTG.

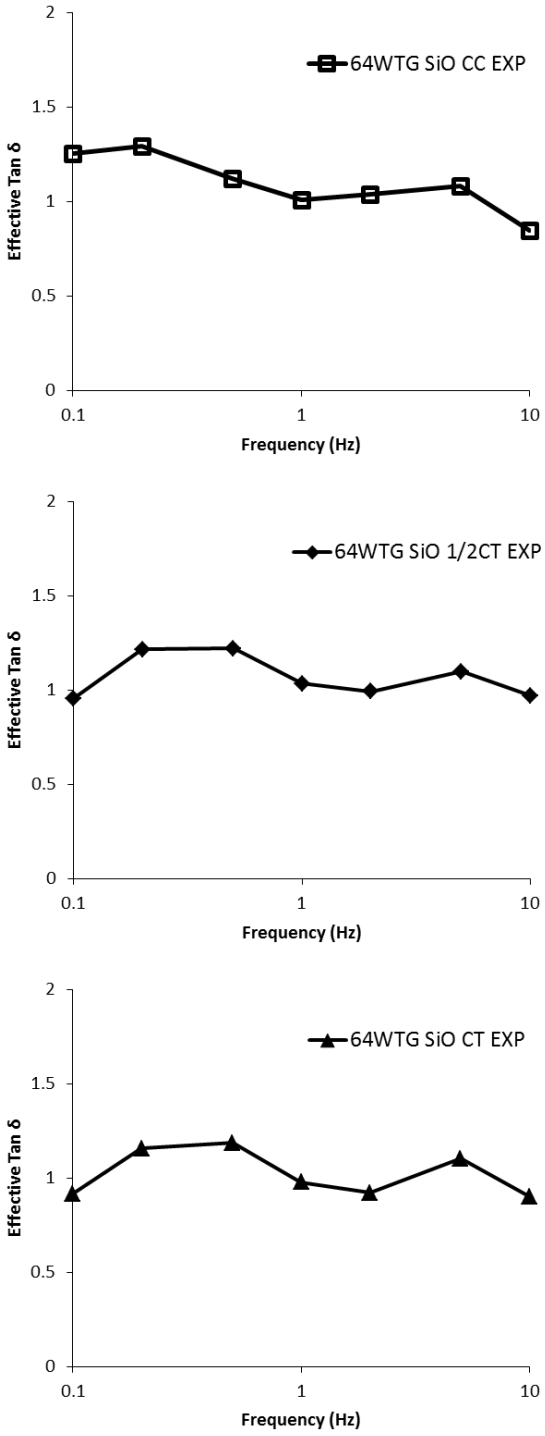

Figure 53. All three strain cases', C/C, 1/2C/T, and C/T from top to bottom, damping shows around one or more tan δs and also exhibits flat region for adaptive damping in the 64WTG with 54vol% SiO-PEG.

5 COMPUTATIONAL ANALYSIS METHODS

5.1 Fluid-Solid Interaction Problem

ANSYS 13 analyzed fluid-solid interaction (FSI) studies. Fluid-solid interaction between the viscous fluid and the hourglass structure is a complex multi-physics problem referred to as a coupled field problem. Transient structure simulation ran without fluids first, and the structure's mesh displacement data transferred into the ANSYS fluid study module, CFX. The pressure data generated by CFX transferred into Transient simulation again for the next time step computation. Solid and fluid domains need different numerical methods: finite element method (FEM) for the solid and finite volume method (FVM) for the fluid. Figure 54 exhibits data flow scheme that shows the connections between solid and fluid module. From the computational simulations, we can analyze three simple viscous and two shear-thinning fluids' damping in 64LHG and suggest a theoretical shear thinning fluid that can produce high passive adaptive damping.

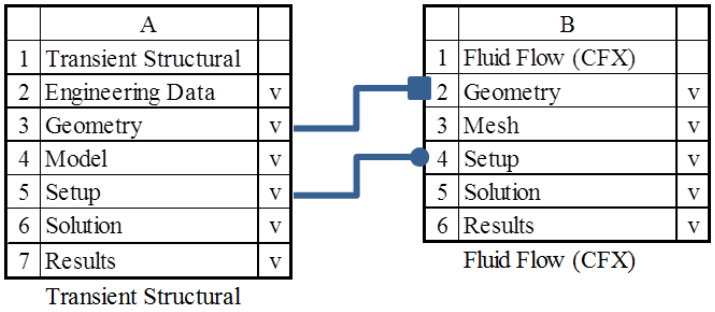

Figure 54. The ANSYS's fluid-solid interaction study runs between Transient Structural and CFX modules (redrawn from [33]).

5.2 Material Properties

The 64LHG structure made by ABS P400 has the homogenized elastic modulus for computations. The 64LHG's dry condition cyclic test produced reaction force 5051 N in the experiment. ANSYS Transient analysis with the calibrated structural elastic modulus, 1.5 GPa, generates the same reaction force 5052.7 N. Poisson's ratio, ν, is 0.35 as the specification indicated. The silicone oil's measured density is 920 kg/m^3 and dynamic viscosities are 100, 60, and 30 Pa·s for each analysis case. Two shear-thinning fluids used in experiments also apply in CFX module. Bird-Carreau law for viscosity can explain the shear-thinning behavior with four variables as presented in equation (9) and Figure 55 [33, 34].

$$\eta = \eta_\infty + (\eta_0 - \eta_\infty)(1 + \lambda^2 \dot{\gamma}^2)^{\frac{n-1}{2}} \quad \textbf{(9)}$$

where

- η is viscosity (Pa·s)
- η_∞ is viscosity (Pa·s)
- η_0 is viscosity (Pa·s)
- λ is natural time (sec) (i.e. Inverse of the shear rate where the fluid starts to show power-law behavior)
- $\dot{\gamma}$ is shear strain rate (sec^{-1})
- n is power-law index

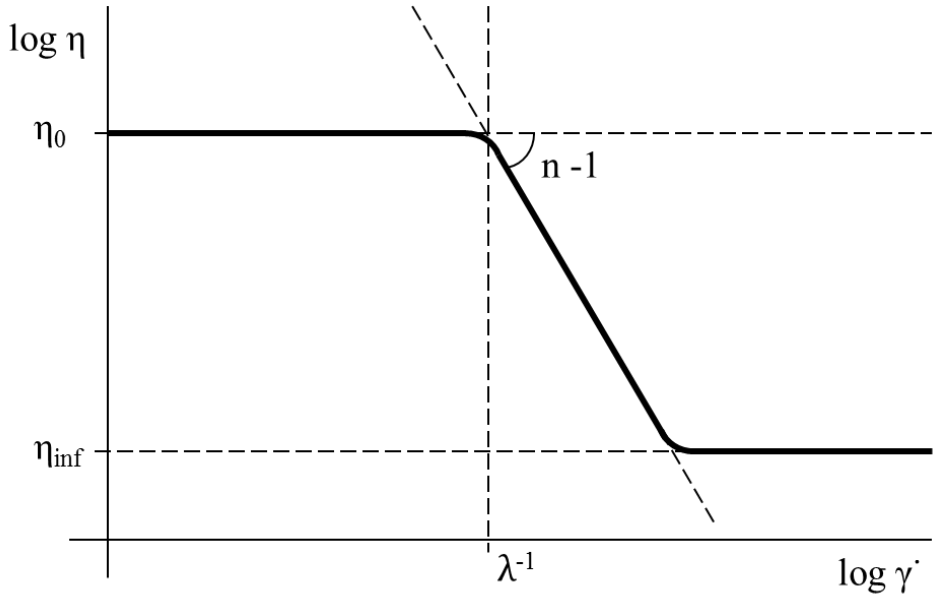

Figure 55. The Bird-Carreau Law for viscosity defines the shear-thinning behavior with four variables (redrawn from [33]).

Table 2 presents 5% PAM-Water solution and 54vol% SiO-PEG's Bird-Carreau variables. Case studies with varying shear-thinning properties found theoretical shear thinning fluid that produce high adaptive passive damping.

Table 2. Bird-Carreau law for viscosity defines two shear thinning fluids, 5% PAM-Water solution and 54 vol% SiO-PEG's shear thinning behaviors.

	5% PAM-Water Solution	54_{vol}% SiO-PEG	
Low Shear Viscosity, η_0	205	500	Pa·s
High Shear Viscosity, η_{inf}	1	1.4	Pa·s
Time Constant, λ	1	625	sec
Power Law Index, n	0.098	0.22	

5.3 Boundary Conditions

Both solid and fluid domains have 10 time steps to compute. For 1 Hz case, the iteration runs every 0.1 second and 10 times for 1 second. The solid domain has quadratic meshes. The 64LHG's Bottom surface is fully constraint in all directions. Top surface applies sinusoidal displacement input in the height direction and fixed the other directions as shown in Figure 56. The Transient structural analysis defines the inner channel surfaces as a Fluid-Solid Interaction condition that exchange pressure and mesh displacement data with the CFX module. The fluid domain has tetragonal meshes, and both opening ends have inflation condition with five layers, 0.77 transition ratio, and 1.2 growth rate. The channel surfaces have no slip conditions. The studies work as laminar flow in room temperature with atmospheric pressure. Unlike experiment conditions, the computational model does not have reservoirs that contain fluids, but the fluid ideally pumps in and out without leaking.

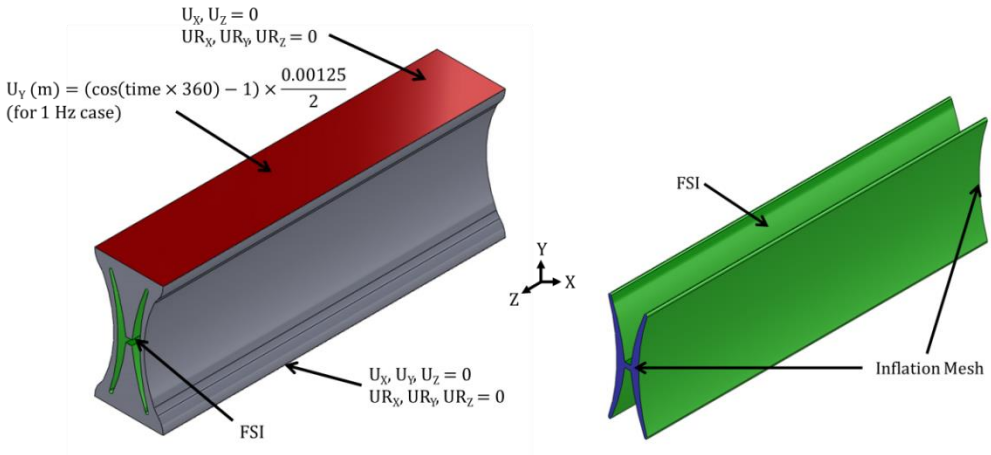

Figure 56. Right depicts solid domain's boundary conditions. The sinusoidal displacement on the top is for 1 Hz case as an example. Left shows fluid domain's boundary conditions.

6 COMPUTATIONAL ANALYSIS RESULTS

6.1 64LHG with Simple Viscous Fluids

The FSI analyzed 64LHG with three high viscous Newtonian fluids that have 100, 60, 30 Pa·s viscosities. The 2% strain on the top surface applied from 0.1 to 5 Hz. The 10 Hz input created cavitation and failed to generate damping. The 100, 60, 30 Pa·s cases produced the peak damping at 1, 5, and 10 Hz, respectively, as shown in Figure 57. This trend that the peak is shifting from right to left by increasing viscosity is the same as experimental results. Discussion section compares experimental and computational results.

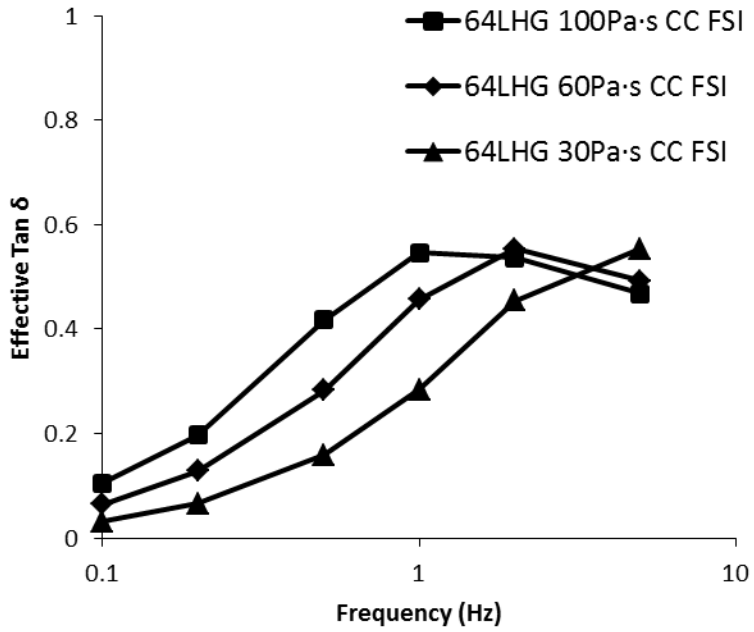

Figure 57. The FSI analyzed 100, 60, and 30 Pa·s viscosity Newtonian fluids

6.2 64LHG with Shear Thinning Fluids

The FSI studies also covered 64LHG's damping with two shear thinning fluids used in the experiments exhibited in Figure 58. The 64LHG with 54vol% SiO-PEG created almost no damping in low frequency range and showed the trend that the damping increased in high frequency range like the experiment. The 64LHG with 5% PAM-Water solution generates 0.14 effective tan δ at 0.1 Hz and shows an increasing trend up to 0.38.

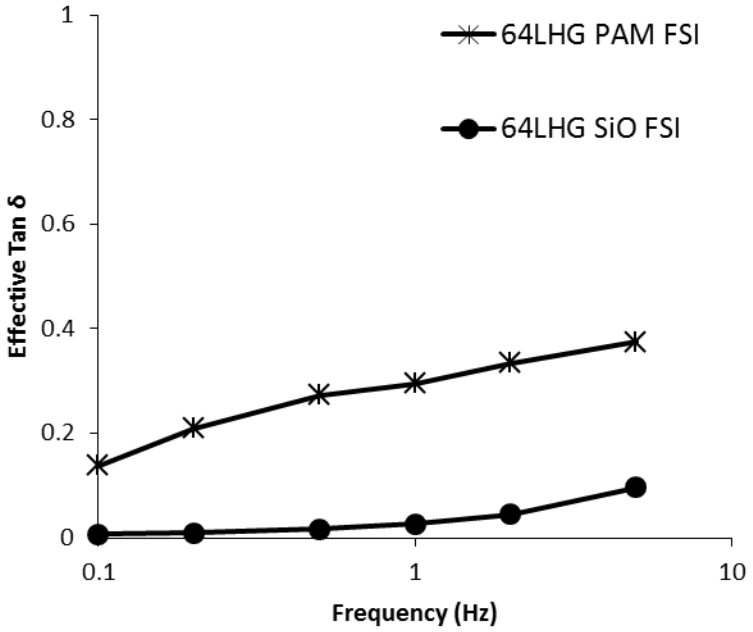

Figure 58. The 5% PAM-Water solution produced damping but no adaptive. The 54vol% SiO-PEG showed almost no damping in low frequency range and increased in high frequency range.

The shear thinning behavior affects adaptive damping as shown in schematic in Figure 59. Left column's two charts exhibits fluid viscosity changes by increasing shear

strain rate, and right column's two plot presents the damping by increasing applied frequencies. The case (A) shows that the shear thinning slop, power law index, affects adaptive behavior. If the fluid is simple viscous fluid that does not change its viscosity by shear strain rate, red line in the left plot, then the damping shows one peak point and dropping behavior on the right chart. The blue line in the left plot is optimum, so the damping plot on the right one shows flat adaptive trend. Below the optimum, the black line on the left chart shows the increasing trend. The fluid adapts better near high frequency range than low area. If the slop is too steep, then the damping on high frequency range is low and shows decreasing trend. The case (B) designates the shear thinning start point, inverse of time constant (λ), also affects adaptive damping. The black line on the left plot is optimum that creates flat damping behavior on the right chart. If the fluid starts shear thinning effect earlier than the optimum, blue line, then the damping shows decreasing trend by increasing frequencies. If the fluid begins shear thinning later than the optimum, red line, it adapts better near higher frequency range and exhibits the increasing trend.

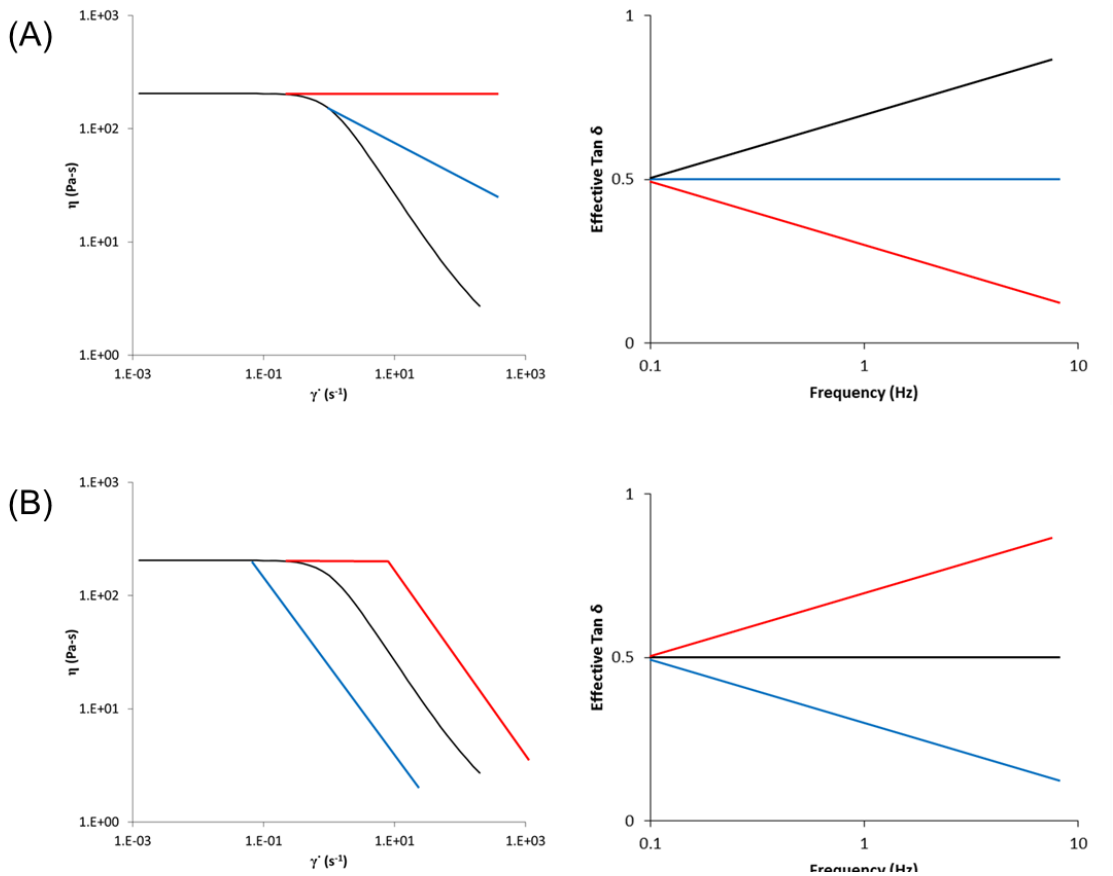

Figure 59. Two of the shear thinning variables, the slop and starting point, affects adaptive damping. Left column's two charts exhibits fluid viscosity changes by increasing shear strain rate, and right column's two plot presents the damping by increasing applied frequencies. Case (A) shows dialing the slop, power law index, effects, case (B) exhibits dialing shear thinning starting point, inverse of time constant, effects.

6.3 64LHG with Theoretical Shear Thinning Fluid

Theoretical shear thinning fluid can produce high passive adaptive damping. Through the case studies, we can find the Bird-Carreau law properties that is η_0: 700 Pa·s, η_∞: 10 Pa·s, λ: 0.667 sec, and n: 0.05. Figure 60 shows the theoretical fluid's shear thinning behavior. The dampings are above simple viscous fluids' one and exhibits adaptive behavior. Figure 61 compares 64LHG FSI results with the theoretical shear

thinning fluid and with the other two shear thinning fluids, 5% PAM-Water solution and 54vol SiO-PEG.

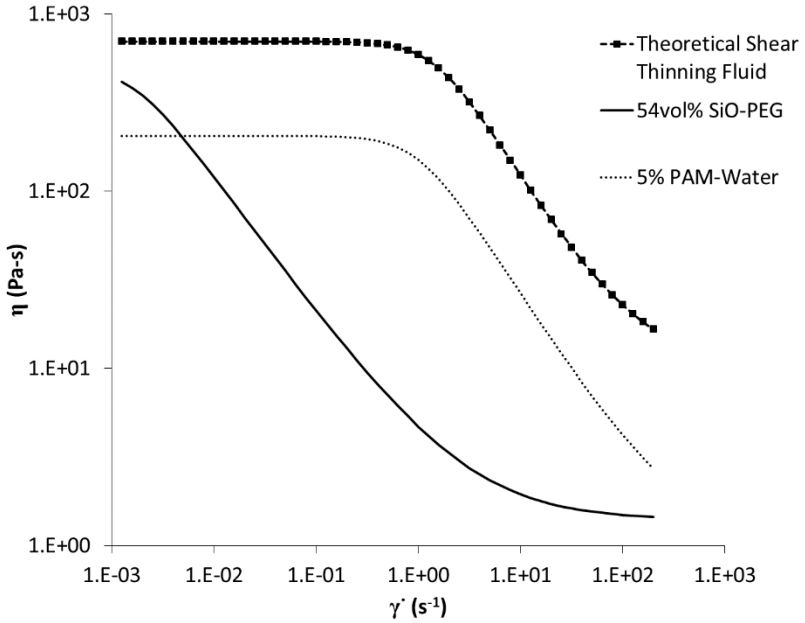

Figure 60. Cases studies helped find theoretical shear thinning fluid's Bird-Carreau law properties shown as square indexes.

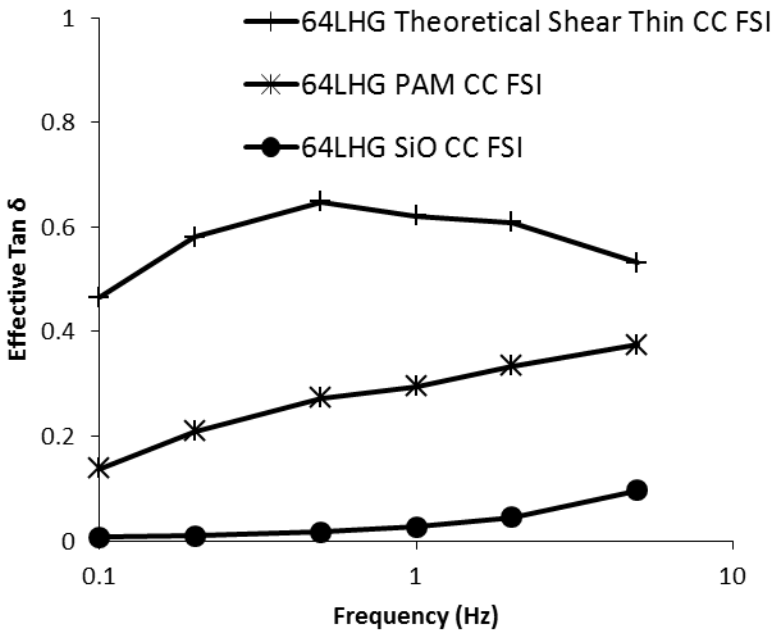

Figure 61. Compared with the other two shear thinning fluids' damping, the theoretical shear thinning fluid obtains high passive adaptive damping.

7 DISCUSSION

7.1 Comparison between Computational Analysis and Experiment

This section discusses and compares results from computational and experimental researches. Left plot shown in Figure 62 is the 64LHG with simple viscous fluids' computational fluid-solid interaction study results, and right one is their experimental results. The peak damping occurs at higher frequency range in computations than in experiments, but the trend that increasing viscosity makes the peak shift to lower frequency range is the same. We can use this trend for passive adaptive damping application. LHGs' serial stacking with various viscous fluids in each layer can generate passively adaptive damping. One LHG layer produces good damping at a frequency, and another LHG layer performs well at another frequency. Overall structure will show good damping through the given frequency range.

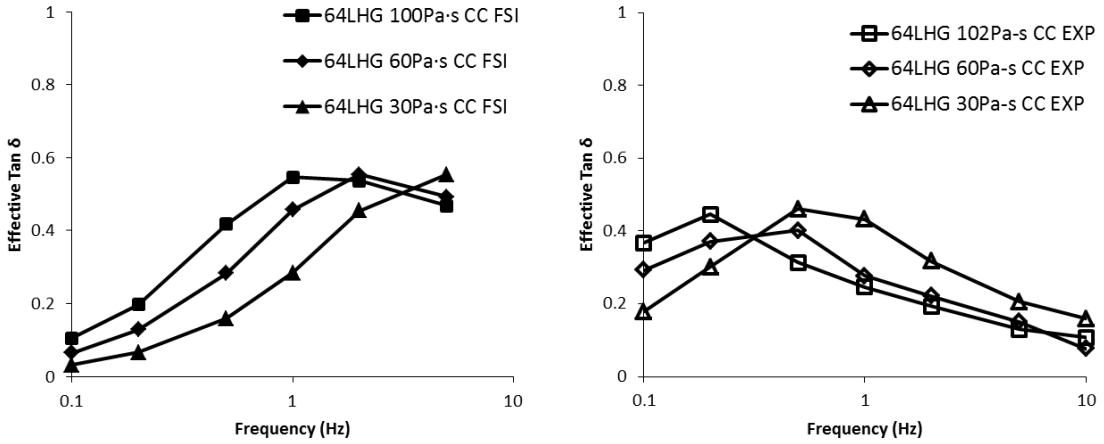

Figure 62. The 64LHG damping with simple viscous fluids in ANSYS analysis (left) and in experiments (right).

The 64LHG with 54vol% SiO-PEG does not show good damping in low frequency range in both computation and experiment as shown in Figure 63 and starts to increase damping after 1 Hz. Like simple viscous studies, experiment's peak damping occurs at lower frequency range in 54vol% SiO-PEG case. Just like simple viscous fluid cases, the damping in the computational analysis result with the shear thinning fluid shows earlier part of damping in the experimental result.

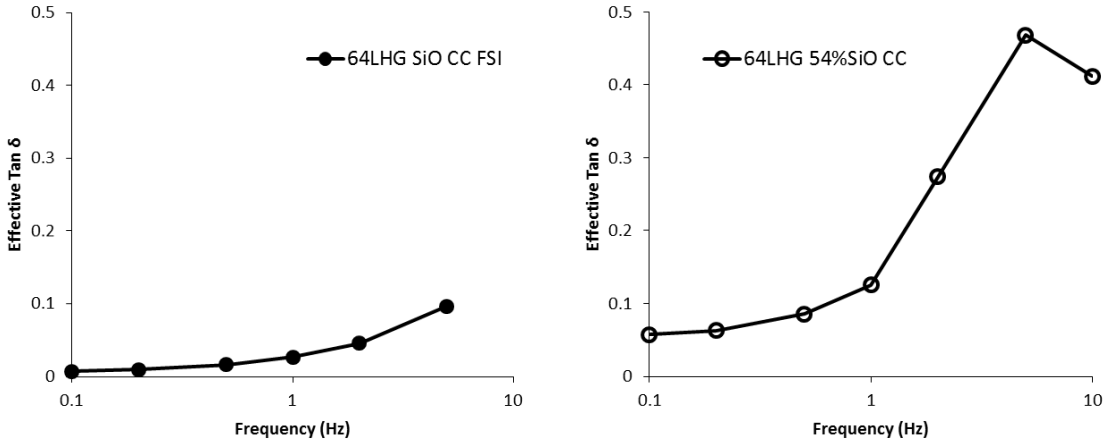

Figure 63. The 64LHG with 54vol% SiO-PEG does not produce good damping in low frequency range in both computation, left, and experiment, right. The damping starts to increase after 1 Hz.

The difference between computations and experiments can be explained with several reasons. Unlike experiments, computational model did not have reservoirs to contain fluid, and pump the fluid in and out ideally. Fluid's rising up against the gravity and lowering down with the gravity through the reservoirs adds energy dissipations by transporting fluid's mass against gravity. Wall condition in computational study was also ideal, no slip. In addition, fluid flow has no turbulence. Turbulence in experiments and small air bubbles in the silicone oil that remains even after degassing process hindered fluid flow that makes differences.

7.2 Improvements in Damping

This research suggests three ways to improve LHG's damping, scaling LHG size down, using a theoretical shear thinning fluid, and reducing the structural elastic modulus.

7.2.1 Scaling LHG Size Down

Scaling down the LHG size can increase the damping as explained in section 3.2.1 and equation (8). Figure 64 compares the results between solo 64LHG with 5% PAM-Water solution and five 16LHG array with S111 elastomer filling in-between the LHGs with 5% PAM-Water solution. The array has more than five times higher damping than 64LHG. Preliminary experiments show scaling down while using the same viscous fluid helps obtain this dramatic increase majorly, rather than adding S111 filling and 16LHG material's structural damping. We can use the scaling effect for obtaining high passive adaptive damping application.

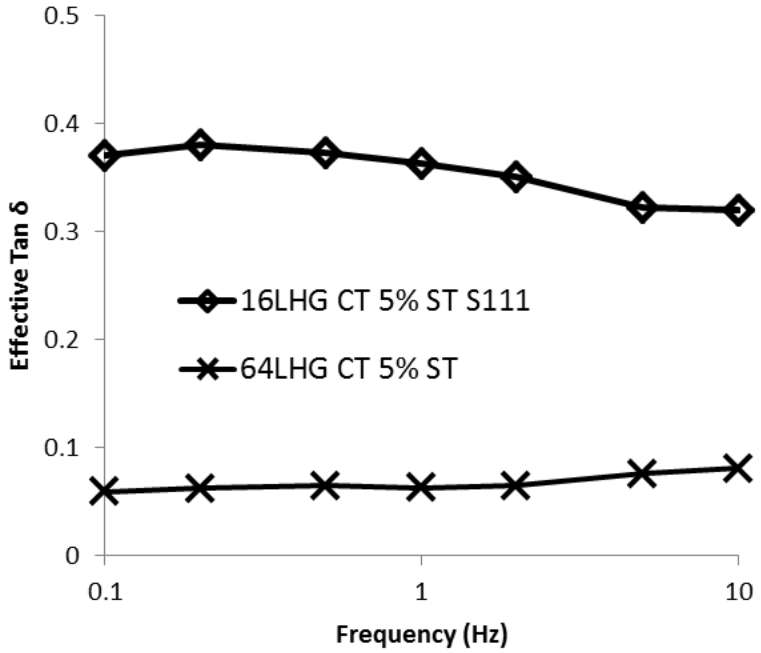

Figure 64. Scaling down from 64LHG to 16LHG makes earn more than five times higher damping because the same viscous fluid flows through narrower channel that is the same effect as increasing fluid's viscosity.

7.2.2 Finding a Theoretical Shear Thinning Fluid

The shear thinning fluids drop its viscosities by increasing frequency that makes right fluid flow for damping. The solo 64LHG's computational data with the theoretical shear thinning fluid can create higher passive adaptive damping than five 16LHG array's experimental data with S111 elastomer filling in-between the LHGs with 5% PAM-Water solution as exhibited in Figure 65. These 64LHG's computational data show the possibility to improve damping by manipulating the fluid's shear thinning properties.

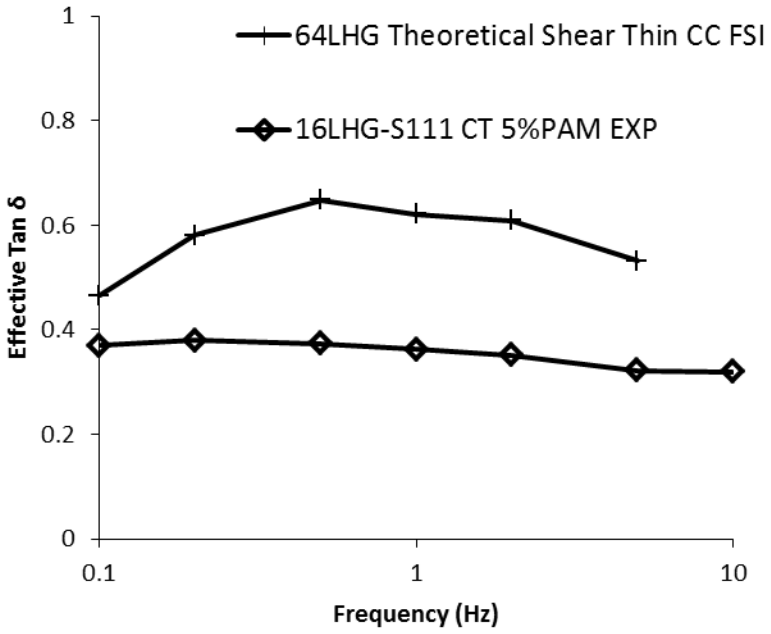

Figure 65. The solo 64LHG's FSI data with the theoretical shear thinning fluid produces higher passive adaptive damping than five 16LHG array's experimental one. This plot shows that manipulating a fluid's shear thinning properties increases damping.

7.2.3 Reducing the Structural Elastic Modulus

The 64WTG reduces stiffness and improve damping because the tan δ is the loss modulus divided by the storage modulus. Figure 66 compares the experimental damping data with 60 Pa·s silicone oil between hourglass structures. The NTG reduced the stiffness by 24% and earned 34% more maximum damping compared with the baseline LHG. The WTG decreased 99% stiffness from the NTG's and gained 54% more maximum damping. The y axis maximum value is 2 tan δ to compare each hourglass at a first glance.

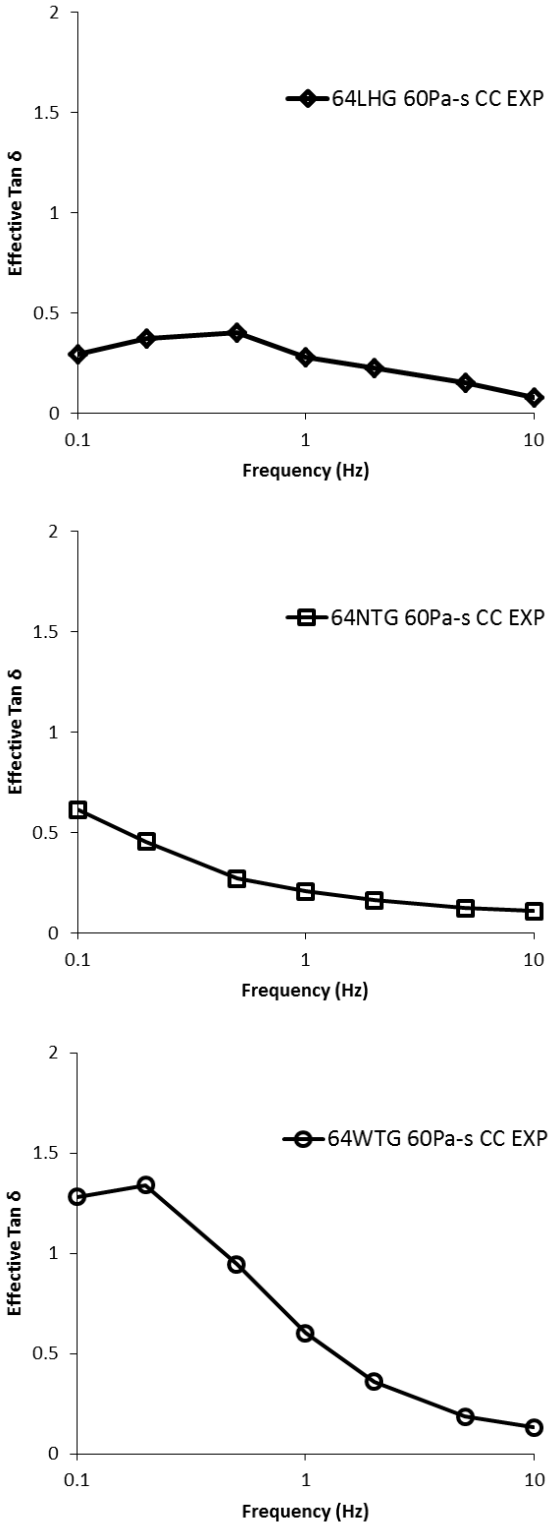

Figure 66. The 64LHG, 64NTG, and 64WTG's damping with 60Pa·s silicone oil shows decreasing stiffness gains in damping. Note: the y axis maximum value is 2 tan δ.

Even though the pumping capability remains in the same, decreasing storage modulus by reducing stiffness makes the tan δ increases. In other words, while keeping the LHG shape as the same, decreasing elastic modulus computationally improve the damping. The 64LHG with 5% PAM-Water solution FSI model decreases its elastic modulus in 15% that increases up to 11% damping as shown in Figure 67.

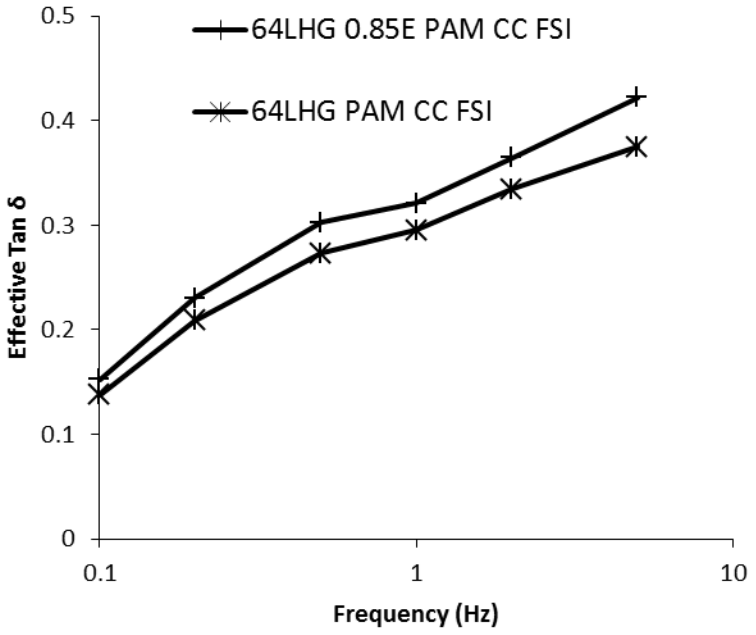

Figure 67. Computational studies show the 64LHG with 5% PAM-Water solution reduces 15% elastic modulus that rises about 10% damping.

8 SUMMARY AND FUTURE WORK

8.1 Summary of Research

This research introduces a novel damping element that works with adaptive composite material. This concept can be a solution1 for vibration in mechanical systems. The damping element, LHG, is a fluid filled damping machine. Cyclic force input from 0.1 to 10 Hz on the LHG's top creates pressure changes in the channel and pumps the fluid in and out. This procedure generates hysteresis behavior that designates damping amount.

Two methods to produce passive adaptive damping are stacking LHGs and using shear thinning fluids. Stacking the LHG layers and using shear thinning fluid can be the solutions to obtain adaptive damping without sensing parts. Multi-layered LHGs with various viscous fluids will show good damping across the given frequency range in overall structure without controlling. Shear thinning infiltrated LHG will perform also good damping in the frequency range. Lower cyclic speed adjusts the shear thinning fluid's viscosity as high by itself to make good fluid flow for damping. Increasing cyclic force input speed causes the viscosity decreasing that creates good damping. Either low or high frequency cyclic inputs generate high damping without additional active control systems.

When improving the pumping capability reaches the limit, tan δ can raise using three methods: scaling LHG size, finding a better shear thinning fluid, and reducing the

structural elastic modulus. If increasing viscosity is limited, the LHG's size can be reduced to produce the increasing viscosity effects. The channel size and viscosity are an inverse proportion relation in Reynolds number analysis. Through the computational fluid-solid interaction studies, the theoretical shear thinning fluid's properties can be obtained that the fluid produces good flow in the LHG channel and creates high passive adaptive damping. The damping, tan δ, is the loss modulus divided by the storage modulus. In the LHGs, the loss modulus and storage modulus are majorly the pumping capability and structural elastic modulus, respectively. Reducing LHG's structural elastic modulus helps gain damping when improving the pumping capability reaches the limit.

8.2 Future Complementary Works

This research's target is to develop a new damping element that will work with negative stiffness element system. The system produces high passive adaptive damping while keeping high stiffness in a given frequency range.

8.2.1 Short HG with Periodic Reservoirs

The hourglass machine can be miniaturized and extruded eventually in the long fiber form. In this case, the fluid travels long distance through the channel and meets the reservoirs at the ends. The fluid's velocity near the middle of hourglass is slow, and the velocity increases toward outlet ends. This large velocity difference creates a viscosity

issue. The fluid near the middle moves slow, so viscosity needs to be high to create damping, but the fluid near outlet will lock in the long fiber channel in the high viscous fluid case. The hourglass with periodic reservoirs in the middle as depicted in Figure 68 can control this issue. This model pumps the fluid toward the periodic reservoirs located in the middle of hourglass.

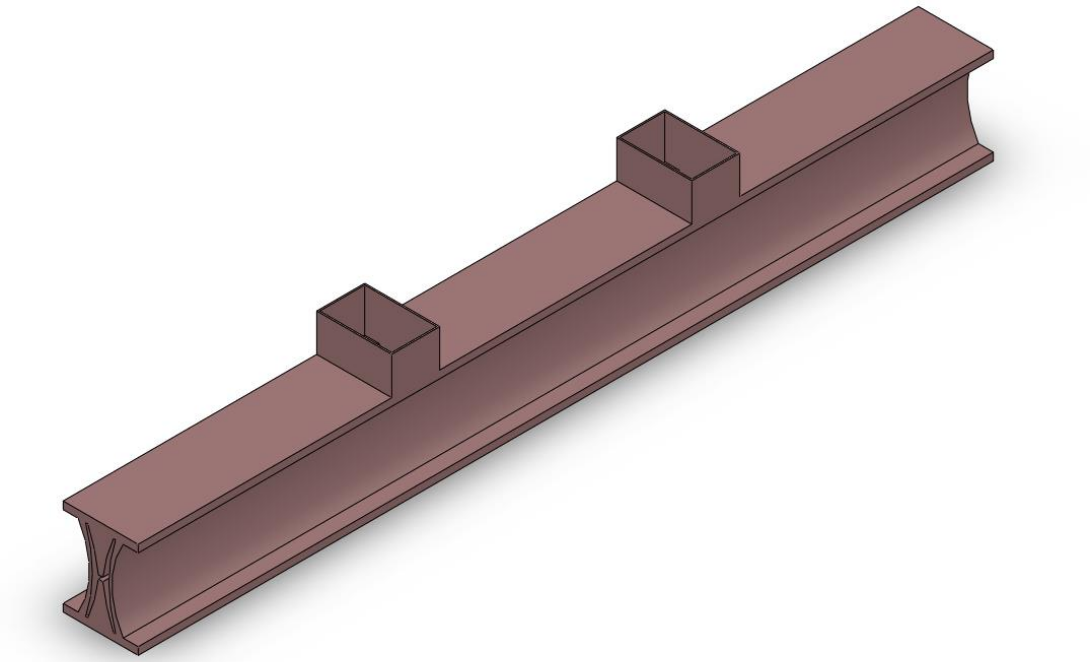

Figure 68. The fluid does not need to travel long distance through the channel, but pumps the fluid toward periodic reservoirs in the middle.

8.2.2 Improvements for LHG

The baseline LHG does not show high passive adaptive damping compared with WTG. Two future research suggestions can solve this issue for the LHG. One future

study can measure the LHG with redesigned geometrical constraint's damping. Making wider geometrical constraints than the baseline LHG's as exhibited in Figure 69 reduces hydraulic radius. The 2% strain makes the channel thin that the sidewalls and geometrical constraints almost touch each other. The pumping ratio is 59% that is 17% higher than baseline LHG's pumping. Moreover, the sidewall shapes are the same as the baseline LHG so that the structural stiffness is the same, 1127 N/mm. This method can increase loss modulus, the numerator of tan δ while keeping storage modulus, the denominator of tan δ. Scaling down and finding ideal shear thinning fluids worked with this redesigned LHG can also be future studies. Because the theoretical shear thinning fluid is specially designed for the baseline LHG's channel, the fluid may not show high performance in the redesigned LHG's channel shape.

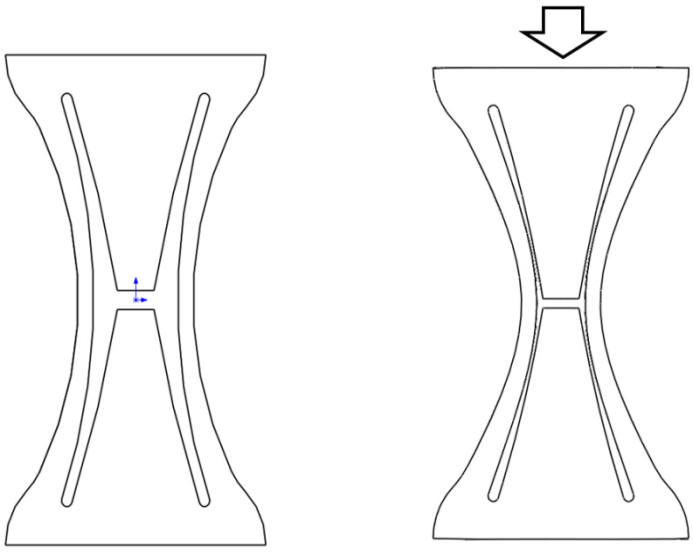

Figure 69. The wider geometrical constraint LHG reduces hydraulic radius that the pumping ratio is 59%. This structure can produce more damping than the baseline LHG.

The other future study is to use a porous material into the LHG's channel. A fluid can wet the material and flow through the pores. The sidewalls squeeze the fluid and pump out of channel in compression phase. In the tension phase, the material recovers its original shape and can be soaked by the fluid again. Even if the fluid's viscosity is not as high as the ideal theoretical shear thinning fluid, an open cell foam creates hindrance for the fluid flow and acts like high viscos fluid's flow.

8.2.3 Improvements for WTG

The 64WTG with 54vol% SiO-PEG shows good adaptive damping but has little structural stiffness, 0.7N/mm. If the negative stiffness element system has high stiffness and the damping part does not need to contribute stiffness, the WTG will be better choice to produce high adaptive damping. The WTG FEA model, however, creates a conversion error because of thinning sidewalls. Hybrid mesh can solve this issue for the future research. We can apply coarse solid meshes to the geometrical constraint parts and fine shell meshes to the thin sidewall sections. This hybrid mesh method can remove the conversion error and reduce computation time.

Adding a positive spring material in between the WTG's geometrical constraints can be tailoring its structural stiffness. The red spring schematic on Figure 70 adds stiffness on the WTG. Dialing the spring's stiffness can control reducing in damping and gaining in structural stiffness.

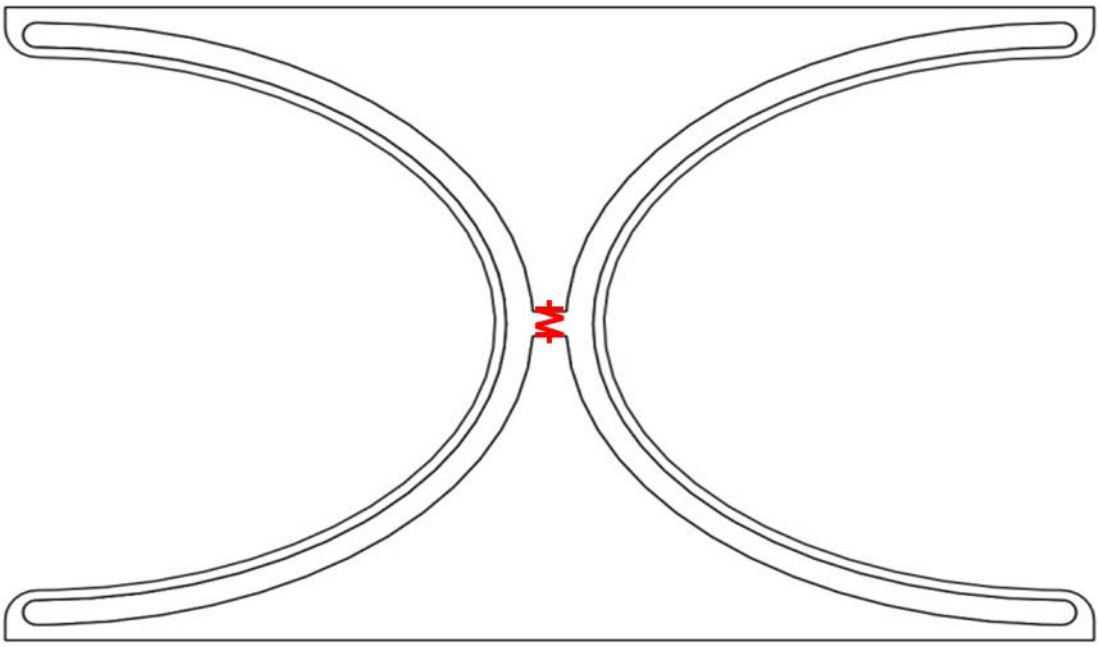

Figure 70. Adding positive spring in between WTG's geometrical constraints can dial its structural stiffness and damping.

8.2.4 Hourglass Application without the Negative Stiffness Element System

The miniaturized LHGs can be extruded as pipe or fiber forms and arrayed into high damping elastomer matrix like a conventional fiber-reinforced composite material form. This composite material can use as automotive panels and aerial vehicle's skin structures. Its unique property that shows high stiffness and passive adaptive damping will compensate a weak point, the fabrication cost. Moreover, simply draining a fluid and inject another can tailor this composite material's structural and damping properties easily. In the future, we can analyze this composite material's mechanical behavior for a specific application.

REFERENCES

1. Kleino, T. D., and Hills, R. "Vibrational Reduction System for Automotive Vehicles." *L&L Products, Inc.*, Romeo, MI, 2003.

2. Thomas, G. R., Fadick, C. M., Fram, B. J., Kirtland, A., and Mexico, N. "Launch vehicle payload adapter design with vibration isolation features," *Proc. SPIE*. Vol. 5760, 2005, pp. 35-45.

3. Lee, Y. T. "Automotive Noise Reduction Material," *blog.naver.com/jin5896847*, 2011.

4. Lakes, R., Lee, T., Bersie, A., and Wang, Y. "Extreme damping in composite materials with negative-stiffness inclusions," *Nature* Vol. 410, No. 6828, 2001, pp. 565-567.

5. Creasy, T. S. "A Proposal Application to DARPA-BAA-10-64 Material Logic," *Technical & Management Proposal*. Vol. I, TEES/TAMU, The Aerospace Corporation, Los Angeles, CA, 2010.

6. Hawkins, G. F., O'Brien, M. J., Zaldivar, R. J., Von Bremen, H. F., and Schurr, J. N. "Development of Machine-Augmented Composites for Infrastructure Applications." The Aerospace Corporation, Los Angeles, CA, 2003, p. 108.

7. Creasy, T. S. "Energy dissipation calculation from hysteresis loop area." Personal Communication, Texas A&M University, College Station, TX, 2011.

8. Tang, C. Y. "Properties and Applications of Machine-Augmented Composites (MACs)," *Aerospace Technical Report*. The Aerospace Corporation, Los Angeles, CA, 2004.

9. Rodriguez, F., Cohen, C., Ober, C., and Archer, L. A. Principles of polymer systems: *Taylor & Francis,* Philadelphia, PA, 1996.

10. McCrum, N. G., Buckley, C. P., and Bucknall, C. B. "Principles of polymer engineering," *Oxford University Press, xii 391,* New York, NY, 1988.

11. Rosen, S. L. Fundamental principles of polymeric materials: *Wiley*, New York, NY, 1982.

12. Chopra, A. K. Dynamics of structures: Theory and applications to earthquake engineering: *Prentice Hall,* Upper Saddle River, NY, 2001.

13. Kim, G., and Singh, R. "A study of passive and adaptive hydraulic engine mount systems with emphasis on non-linear characteristics," *Journal of Sound and Vibration* Vol. 179, No. 3, 1995, pp. 427-453.

14. Khorrami, F., Rastegar, J., and Erwin, R. S. "A three degrees-of-freedom adaptive-passive isolator for launch vehicle payloads," *Proceedings of SPIE*. Vol. 3991, 2000, pp. 164-175.

15. Sperling, L. H. Introduction to physical polymer science: *Wiley-Interscience*, Princeton, NJ, 2005.

16. Kim, J. "Passive machine augmented composite for multifunctional properties," *Mechanical Engineering*. Ph.D., Texas A&M University, College Station, TX, 2005.

17. Lazan, B. J. Damping of materials and members in structural mechanics: *Pergamon Press*, Elmford, NY, 1968.

18. Cremer, L., Heckl, M., and Petersson, B. A. T. Structure-borne sound: structural vibrations and sound radiation at audio frequencies: *Springer*, Berlin, Germany 2005.

19. Lakes, R. L. S. Viscoelastic Solids: *CRC Press*, Boca Raton, FL, 1999.

20. Janmey, P. A., Georges, P. C., and Hvidt, S. "Basic Rheology for Biologists," *Methods in Cell Biology*. Vol. 83, Academic Press, 2007, pp. 1-27.

21. Shaw, A., Neild, S., Wagg, D., Weaver, P., and Carrella, A. "Experimental Investigation into a Passive Vibration Isolator incorporating a Bistable Composite plate," *54th AIAA/ASME/ASCE/AHS/ASC Structures, Structural Dynamics, and Materials Conference*. Vol. 2013, AIAA, Boston, MA, 2013.

22. Platus, D. L. "Negative-stiffness-mechanism vibration isolation systems," *San Jose-DL tentative*. International Society for Optics and Photonics, 1992, pp. 44-54.

23. Hawkins, G. F. "Augmenting the mechanical properties of materials by embedding simple machines," *Journal of Advanced Materials* Vol. 34, No. 3, 2002, pp. 16-20.

24. McCutcheon, D. M. "Machine augmented composite materials for damping purposes," *Mechanical Engineering*. M.S., Texas A&M University, College Station, TX, 2004.

25. Schwille, J. A. "New trial hourglass machine geometry." The Aerospace Corp, Los Angeles, CA, 2011.

26. NASA. "Reynolds Number," NASA Glenn Research Center, 2009.

27. Brookfield. "General Purpose Silicone Fluids," www.brookfieldengineering.com/products/viscosity-standards/general-purpose-silicone-fluids.asp, 2013.

28. Haycock, R. F., Caines, A. J., and Hillier, J. E. Automotive lubricants reference book: *John Wiley & Sons*, Warrendale, PA, 2004.

29. Anan, "Silicone oil," *Sigma-Aldrich Co. LLC.* , 2013.

30. Kreiba, A. "The rheological properties of aqueous polyacrylamide solutions," *Mechanical Engineering*. M.S., Concordia University, Austin, TX, 2000.

31. van Krevelen, D. W., and te Nijenhuis, K. Properties of Polymers: Their correlation with chemical structure; their numerical estimation and prediction from additive group contributions: *Elsevier Science*, Oxford, UK, 2009.

32. Lim, A. S., Lopatnikov, S. L., Wagner, N. J., and Gillespie, J. W. "Investigating the transient response of a shear thickening fluid using the split Hopkinson pressure bar technique," *Rheologica Acta* Vol. 49, No. 8, 2010, pp. 879-890.

33. Ansys CFX "ANSYS User's Manual." www.ansys.com/Products/ANSYS+14.5+Release+Highlights, 2013.

34. Matolcsi, K., Bárdossy, G., and Halász, G. "Simulation of Saline Solution Injection into a Venous Junction," *5th European Conference of the International Federation for Medical and Biological Engineering*. Vol. 37, *Springer*, Budapest, Hungary, 2012, pp. 343-346.